Politecnico di Torino

Politecnico di Torino

Master Degree course in Land and Environmental Engineering, Climate Change

A.a. 2024/2025

Graduation Session March 2026

Sources of predictability of intense European summer droughts from SEAS5 ECMWF forecasts

Supervisor
Prof. Jost-Diedrich Graf Von Hardenberg

Candidate
Francesco Contarino

Co-supervisor
Giada Cerato

Abstract

Europe is currently experiencing an increase in the severity and frequency of summer droughts driven by global warming. Forecasting these seasonal events months in advance is a crucial tool for effective environmental planning and the mitigation of environmental and socio-economic impacts. However, accurate prediction of European summer droughts remains a significant challenge for seasonal forecast models. This thesis aims to investigate the predictive skill and sources of predictability of the fifth-generation seasonal forecast system (SEAS5), developed by ECMWF, regarding summer drought events in Europe. To detect and quantify these events, the Standardized Water Balance Anomaly (SWBA) index was employed. This index is derived from the atmospheric water balance—the difference between precipitation and potential evapotranspiration. The analysis focuses on four intense European summer droughts: two poorly predicted by the model (2003 and 2015) and two more accurately predicted (2018 and 2022). These case studies are selected because, among all the observed drought summers, they are characterized by particularly high and low area-weighted average Brier Score (BS), respectively. The BS is calculated exclusively over the regions that effectively experienced a drought according to observational data, serving as a robust statistical indicator of forecast accuracy. For each case study, anomalies of five key climate variables— soil moisture, 2-meter air temperature, total precipitation, mean sea level pressure, and sea surface temperature—are computed with respect to the 1993–2016 climatological mean, utilizing both ERA5 observational data and SEAS5 model outputs. The comparison between observed anomalies and SEAS5 predictions, combined with a significance test performed on both the best- and worst-performing ensemble members regarding the summer water balance, reveals critical links between the model's performance and specific co-occurring atmospheric or oceanic circulation patterns. Notably, the results highlight a systematic limitation in the model's ability to resolve complex blocking high-pressure systems, particularly those occurring over Europe under negative Summer North Atlantic Oscillation (SNAO) phase. Consequently, SEAS5 proves to be significantly more skilful in predicting drought seasons characterized by a positive SNAO.

Table of Contents

Abstract II

List of Figures VI

1 Introduction 1
- 1.1 The concept of drought . . . 1
- 1.2 Droughts in Europe . . . 4
- 1.3 Seasonal Forecasts . . . 5

2 Data and Models 7
- 2.1 Observational data: ERA5 and HadiSST . . . 7
- 2.2 Seasonal forecasts data: SEAS5 . . . 10

3 Methodology 15
- 3.1 Water balance . . . 15
- 3.2 Standardized Water Balance Anomaly . . . 16
- 3.3 Brier Score . . . 18
- 3.4 Climatological Anomalies . . . 19
- 3.5 Significance Test . . . 21
- 3.6 SNAO Index . . . 23

4 Results 25
- 4.1 Water Balance and Brier Score Time Series . . . 26
- 4.2 SWBA and BS . . . 32
- 4.3 Climatological Summer Anomalies . . . 40
  - 4.3.1 Soil Moisture . . . 41

4.3.2 Air temperature at 2 metres 44
4.3.3 Total Precipitation 49
4.3.4 Mean Sea Level Pressure 53
4.3.5 Sea Surface Temperature 62

5 Discussion 69

6 Conclusion 77

References 79

List of Figures

4.1 (a)Interannual variability of the accumulated European Summer Water Balance derived from ERA5 reanalysis [1981,2022]. Text box displays the mean of the accumulated European Summer Water Balance of the entire period [1981,2022], the specific values for the four summers under study and the p-value of the trend, which shows great significance of the observed trend (**, p-value < 0.01).(b)Spatial distribution of the accumulated Summer Water Balance trend based on ERA5 reanalysis calculated over the period [1981,2022]. Stippling indicates statistical significance at the 95% level (p value < 0.05). . 26

4.2 Interannual variability of the Brier Score for European summer drought prediction. The score is computed exclusively for the European grid points where drought was observed according to the ERA5 Reanalysis. Text box displays the area-weighted average Brier Score computed both for the entire period [1981,2022] and for the four summers under study taking into account only the grid points where the summer drought was recorded according to ERA5 data. Text box displays also the P-PET value related to each summer. Red dots in the time series indicate the poor-predicted summers of 2003 and 2015, while green dots indicate the well-predicted ones of 2018 and 2022. 29

4.3 JJA Standardized Water Balance Anomaly for the target drought years relative to the 1993–2016 climatology. Left column (a–d): ERA5 reanalysis; Right column (e–h): SEAS5 ensemble mean. . . . 32

4.4 Observed (left, a-d) and predicted (right, e-h) drought areas (red pixels) for the target summers [2003, 2015, 2018, 2022]. Observed drought areas refer to ERA5 reanalysis dataset. Predicted drought areas refer to the SEAS5 ensemble mean. Text box displays the number of red grid points which are affected by drought conditions. 35
4.5 SEAS5 forecast probability of summer drought conditions for the target years. Text boxes display the mean probability computed considering all the grid points of the domain. 37
4.6 Spatial distribution of the Brier Score for SEAS5 Summer drought predictions. Text boxes display the Mean BS computed considering only the grid points of the domain where the drought occurred. . . 38
4.7 May Soil Moisture Anomalies relative to the 1993–2016 climatology for the target years [2003, 2015, 2018, 2022]. (left column, a–d) ERA5 reanalysis; (right column, e–h) SEAS5 ensemble mean. 41
4.8 JJA 2m Air-temperature Anomalies relative to the 1993–2016 climatology for the target years [2003, 2015, 2018, 2022]. (left column, a–d) ERA5 reanalysis; (right column, e–h) SEAS5 ensemble mean. . 44
4.9 Driest (left column, a-d) and Wettest (right column, e-h) SEAS5 members t2m JJA Anomalies. Stippling indicates statistical significance at the 95% level (p value < 0.05). 45
4.10 JJA Total Precipitation Anomalies relative to the 1993–2016 climatology for the target years [2003, 2015, 2018, 2022]. (left column, a–d) ERA5 reanalysis; (right column, e–h) SEAS5 ensemble mean. . 49
4.11 Driest (left column, a-d) and Wettest (right column, e-h) SEAS5 members Tp JJA Anomalies. Stippling indicates statistical significance at the 95% level (p value < 0.05). 50
4.12 JJA Mean Sea Level Pressure Anomalies relative to the 1993–2016 climatology for the target years [2003, 2015, 2018, 2022]. (left column, a–d) ERA5 reanalysis; (right column, e–h) SEAS5 ensemble mean. . 53
4.13 Driest (left column, a-d) and Wettest (right column, e-h) SEAS5 members MSLP JJA Anomalies. Stippling indicates statistical significance at the 95% level (p value < 0.05). 54

4.14 SEAS5 ensemble spread for the SNAO index forecast for the four target years. Red stars indicate the recorded SNAO index according to ERA5 reanalysis. Text box exhibits the percentage of members predicting SNAO < 0, $0 <$ SNAO < 1, and SNAO> 1 for the target summers. 59
4.15 JJA Sea Surface Temperature Anomalies relative to the 1993–2016 climatology for the target years [2003, 2015, 2018, 2022]. (left column, a–d) HadiSST observations; (right column, e–h) SEAS5 ensemble mean. 62
4.16 Observed (HadiSST) May SST anomalies relative to the 1993–2016 climatology for the target years [2003, 2015, 2018, 2022]. 65
4.17 SST Driest - Wettest SEAS5 members. Stippling indicates statistical significance at the 95% level (p-value < 0.05). 66

Chapter 1

Introduction

1.1 The concept of drought

According to the World Meteorological Organization (WMO)'s definition, droughts are prolonged dry periods within the natural climate cycle. They are natural phenomena that can occur in all types of climates worldwide and are related to a reduction or total absence of rainfall over an extended period, typically lasting a season or longer (Dai, 2011). Although droughts are inherently linked to rainfall shortages, several other climatic factors—such as high temperatures, strong winds, and low relative humidity—contribute to worsening their effects (Wilhite & Svoboda, 2000). Often, this leads to water deficiencies across various elements of the hydrological cycle—ranging from soil moisture to streamflow and groundwater reservoirs—causing severe problems to water supply and agriculture (Van Loon & Laaha, 2015).

Wilhite & Svoboda, (2000) highlight that droughts do not depend solely on the total amount of rainfall, but also on its timing. In other words, a drought event can arise from delays in the rainy season, negatively affecting agriculture if wet periods occur out of phase with critical crop growth stages. Moreover, droughts can alter precipitation patterns, resulting in fewer but more intense rainfall events; this negatively impacts the water cycle, agriculture, and ecosystems, even if the total seasonal rainfall remains consistent with ordinary values (Knapp et al., 2008).

The complexity and interdisciplinary nature of the phenomenon led Wilhite &

Glantz (1985) to formulate four distinct categories to define droughts and their effects: Meteorological, Agricultural, Hydrological, and Socio-economic. These categories are useful for understanding the different dimensions of drought. A drought is classified as Meteorological when it is defined by its degree of dryness, the duration of the dry period, and specific atmospheric parameters such as precipitation or temperature. However, meteorological definitions encountered inconsistencies when attempting to establish absolute thresholds valid across all climate types; to address this issue, several internationally recognized indices have been developed over the years, such as the Palmer Drought Severity Index in 1965, the Standardized Precipitation Index (SPI) formalized in 2009, and the Standardized Precipitation Evapotranspiration Index (SPEI) in 2010.

Agricultural droughts, on the other hand, are detected by assessing crop health. They are closely connected to meteorological droughts, as the soil moisture necessary for proper crop growth is directly linked to the amount of precipitation and the rate of evapotranspiration. The Crop Moisture Index quantifies the severity of an agricultural drought by computing the difference between actual and expected weekly evapotranspiration. Additionally, the severity of this type of drought is heavily influenced by its timing relative to the different phenological phases of crop growth.

Hydrological droughts are measured based on their impacts on the regional hydrological cycle, particularly concerning river basins and both surface and subsurface flows. They do not occur simultaneously with meteorological and agricultural droughts, as their effects on the broader hydrological cycle take longer to manifest. Typically, this type of drought is measured through runoff monitoring or by using the Surface Water Supply Index, which considers reservoir storage, streamflow, and high-elevation precipitation, comparing them against historical baseline data.

Finally, Socio-economic droughts are strongly interconnected with the other types, as they evaluate the supply and societal demand of economic goods primarily related to agriculture and freshwater resources.

In 2017, Crausbay et al. coined a further definition: the Ecological drought. According to the authors, the severity of a dry event can also be determined by measuring the negative impacts of water deficits on ecosystems, thereby identifying specific vulnerability thresholds.

What distinguishes droughts from other climatic hazards is the complexity involved in precisely assessing their onset and effective end. This concept is well explained by Tannehill in his 1947 book “Drought: Its Causes and Effects”, where the author defines drought as a "creeping phenomenon": its effects build up gradually over a long period and can persist for years even after the meteorological event has ended. Furthermore, droughts typically affect much wider geographical areas—often encompassing entire regions—compared to the majority of natural hazards, such as floods or hurricanes, whose impacts are generally more localized and easier to detect. The combination of these two characteristics highlights the inherent complexity in managing and monitoring this climatic hazard.

In recent years, several international policies have been drafted to define droughts. The SPI was officially recognized in 2009 by the WMO as the standard index for establishing precipitation-based thresholds for drought detection. This index was subsequently expanded the following year by Vicente-Serrano with the introduction of the SPEI, which incorporates temperature and evapotranspiration into its computation. For the purpose of this thesis, the Standardized Water Balance Anomaly (SWBA) will be employed, which shares its physical foundation with the aforementioned SPEI, and has proven to be a robust alternative to the latter for evaluating drought severity (e.g., Jiao et al., 2021). Indeed, they both rely on the climatic water balance—defined as the difference between precipitation and potential evapotranspiration—capturing the combined effects of rainfall shortages and increased atmospheric evaporative demand. However, they differ in their statistical standardization procedures. While the classic SPEI involves fitting a complex, three-parameter log-logistic probability distribution to the data, the SWBA relies on a direct Z-score standardization on raw data. Rather than fitting a theoretical probability distribution, the SWBA standardizes the seasonally accumulated water balance using the mean and standard deviation calculated directly from the reference climatology.

This methodological choice was made to address the challenges of analyzing the 51-member SEAS5 ensemble. Applying a log-logistic fit to each individual ensemble member would be computationally too complex. By employing the SWBA, it was possible to compute the anomaly for each member of the ensemble.

1.2 Droughts in Europe

It is well established that anthropogenic forcings are affecting the global climate, as emissions of CO2 and other greenhouse gases into the atmosphere are leading to a concerning rise in global temperatures (Lindsey et al., 2020). Driven by the Clausius-Clapeyron relationship, higher temperatures exponentially increase the moisture-holding capacity of the air. This widens the vapor pressure deficit and increases atmospheric evaporative demand, which exacerbates moisture deficits and results in more frequent and extreme droughts (Vicente-Serrano et al., 2014). Furthermore, a more moisture-demanding atmosphere serves as a primary driver for the intensification of hydrological extremes (Dai, 2013). A study conducted by Dai in 2011 explained that over the last century, "global aridity and drought areas have increased substantially". Particularly, during the last century, the frequency and severity of drought events in Europe have risen significantly due to changes in atmospheric patterns driven by global warming, making droughts a continental-scale hazard (Hanel et al., 2018).

Although the Mediterranean basin remains the primary hotspot for drought risk, this exposure has significantly expanded into almost all parts of Europe due to changes in atmospheric dynamics (Cresswell-Clay et al., 2022). Cresswell-Clay et al. (2022) explains that the poleward expansion of the Hadley cell, driven by global warming, is causing the Azores High to expand towards the northeast, which in turn leads to drier winters, especially across southwestern Europe. This is a serious issue considering that winter rainfall and snow accumulation in the Alps and the Pyrenees are vital for the region's ecological and economic health (Cresswell-Clay et al., 2022). For instance, during the winter of 2021–2022, a persistent high-pressure ridge resulted in an anomaly of 88% in peak snow water equivalent, along with intraseasonal snowmelt and earlier melt-out dates; these factors led to the lowest terrestrial water storage on record in the Po basin during the summer of 2022 (Avanzi et al., 2024).

Additionally, Arctic amplification is playing a detrimental role in enhancing drought conditions across the European continent (Cohen et al., 2014). The Arctic is warming faster than the equator, diminishing the temperature gradient that drives the jet streams in the mid-latitudes. The weakening of these fast-moving air

currents, which typically steer Atlantic storms across the continent, can result in more persistent weather patterns where high-pressure systems become stationary for weeks (Cohen et al., 2014). These stagnant anticyclones deflect rain-bearing storms and trap heat, creating heat domes that effectively bake the soil (Miralles et al., 2019). The severe drought registered in Europe during the summer of 2022 appears to have been caused by the persistence of high-pressure systems linked to the atmospheric blocking phenomena just described (Garrido-Perez et al., 2024).

Climate change is not only modifying global atmospheric patterns, but it is also increasing the frequency of rare events, particularly concerning droughts. The IPCC (2022) confirmed that under current climate warming scenarios, the frequency of extreme droughts is projected to double in Western and Central Europe and potentially triple in the Mediterranean, making water scarcity a chronic rather than an episodic condition for a significant portion of the continent.

1.3 Seasonal Forecasts

As droughts occur on a seasonal timescale, seasonal forecasts represent one of the most effective tools for their prediction. Seasonal forecasts provide a broad overview of atmospheric evolution over a 7-month or 12-month forecast period (Stockdale, 2021). They are fundamentally probabilistic in nature, identifying a variety of potential climate evolutions (Calì Quaglia et al., 2022).

The European Centre for Medium-Range Weather Forecasts (ECMWF) (Stockdale, 2021) defines them as a "statistical summary of the daily weather calculated by the forecast model in the months ahead". These coupled land-ocean forecasts bridge the gap between short-term weather forecasts and long-term climate projections (Troccoli, 2010). Their long-range predictability arises from the slowly varying elements within the climate system (Troccoli, 2010). Examples of these elements include sea surface temperatures—which change gradually due to the large heat capacity of the oceans—snow cover, sea ice, and various other land surface processes (Krishnamurthy et al., 2019). The interaction between these slowly varying boundary conditions and the atmosphere's initial conditions can generate predictable phenomena characterized by longer timescale variations (Krishnamurthy et al., 2019).

Overall, the long-term predictability of oceanic patterns at the monthly scale, which exert a significant global impact on atmospheric circulation, justifies the reliability of seasonal forecasts (Copernicus Climate Change Service, 2026). Across equatorial and tropical regions, the coupling between the atmosphere and the ocean is stronger, making seasonal forecasts generally more successful at low latitudes. Outside of these regions, the skill and efficiency of these models can decrease significantly (Calì Quaglia et al., 2022).

This study focuses on Europe, a mid-latitudes region where seasonal forecasting remains highly challenging and where an in-depth analysis of the skills and constraints of current seasonal models is essential for their future improvement (Calì Quaglia et al., 2022). Notably, Cerato et al. (2025) highlight how seasonal forecasts models better predict summer droughts indicators over Mediterranean region compared to Northern Europe. This spatial variability is mainly attributed to the different drivers of drought, as the evolution of summer droughts in Northern Europe is primarily dictated by precipitation, which is less predictable than temperature (Cerato et al., 2025).

In this context, this study aims to assess the accuracy of summer drought forecasts provided by the fifth-generation seasonal forecast system (SEAS5) developed by the ECMWF. For this purpose, the Brier Score (BS) is calculated as the primary measure of accuracy. Four dry summers (2003, 2015, 2018, and 2022) were chosen as crucial case studies due to their low water balance values and their contrasting BS results, which indicated low accuracy for the 2003 and 2015 events and high accuracy for 2018 and 2022. The climatological features of such events will be analysed and compared to identify potential sources of predictability.

Chapter 2

Data and Models

This thesis utilizes data distributed by ECMWF, specifically ERA5 for the observational baseline and SEAS5 for the seasonal forecasts. The only exception is the sea surface temperature observational data, which were extracted from the HadiSST (Hadley Centre Global Sea Ice and Sea Surface Temperature) historical dataset. The variables employed in the analysis include soil moisture, maximum and minimum daily 2-meter temperatures, mean 2-meter air temperature (t2m), total precipitation (tp), mean sea level pressure (MSLP), and sea surface temperature (SST). The selection of these specific variables is grounded in the framework of compound climate extremes.

2.1 Observational data: ERA5 and HadiSST

ECMWF is an intergovernmental organization supported by the majority of European countries. It produces global numerical weather forecasts maintaining one of the largest meteorological data archives in the world (ECMWF, 2026).

The acronym ERA5 stands for ECMWF ReAnalysis (version 5); it is the fifth generation of atmospheric reanalyses produced by the ECMWF, providing hourly estimates for numerous meteorological variables from January 1940 to the present day, with near real-time updates (ECMWF, 2026). ERA5 is a high-resolution reconstruction of historical weather data that fills the spatial and temporal gaps inherent in observational data through the Integrated Forecasting System. This

system contains a sophisticated data assimilation framework and a comprehensive global numerical model of the Earth system.

The ERA5 dataset covers the Earth on a 31 km grid, and the atmosphere is vertically resolved using 137 levels ranging from the surface up to an elevation of 80 km (ECMWF, 2026). Unlike the SEAS5 system, ERA5 does not utilize a three-dimensional ocean model with vertical depth levels. Instead, it couples the atmospheric model with a Wave Model (WAM) (Hersbach et al., 2020).

The aforementioned variables needed for this study were originally available at a spatial resolution of 0.25°x0.25°. We performed a bilinear interpolation to upscale them to 1°x1° resolution, matching the SEAS5 grid.

In the bilinear interpolation method, to determine the value of a newly defined larger pixel, the algorithm selects the four closest original pixels from the ERA5 grid and calculates a weighted average based on their relative distance. The rationale behind this methodological choice is to achieve standardization and consistency, thereby allowing for a direct comparison between the observational baseline and the forecast variables. It should also be noted that the original hourly data can be aggregated into daily or monthly intervals, which results in datasets that are computationally lighter and more manageable for long-term analyses.

As previously stated, observational data for SST were extracted from the HadiSST dataset provided by the Met Office Hadley Centre. HadiSST is the combination of monthly globally complete fields of SST and sea ice concentration from 1871 to present (Rayner et al., 2003). Unlike ERA5 Reanalysis dataset, HadiSST is a historical observational dataset which reconstructs global ocean surface conditions by collecting in situ measurements from ships and buoys, later integrated with satellite-derived data from 1982 onwards. It has a horizontal resolution of 1°x1° (no further interpolation is needed to match the spatial grid of the SEAS5 seasonal forecast outputs). Tables 2.1 and 2.2 shown below exhibit the observational data description from these two different datasets.

ERA5	
Data type	Gridded
Projection	Regular latitude-longitude grid
Horizontal coverage	Global
Horizontal resolution	**Atmosphere:** 0.25°× 0.25° (∼28 km)
Vertical resolution	**Atmosphere:** 137 levels (up to 80 km)
Temporal coverage	1940 to present
Temporal resolution	Hourly
File format	NetCDF
Update frequency	Daily

Table 2.1: ERA5 Data description from Climate Data Store (CDS) Copernicus.eu.

HadiSST	
Data type	Gridded
Projection	Regular latitude-longitude grid
Horizontal coverage	Global
Horizontal resolution	**Ocean:** 1°× 1° (∼100 km)
Temporal coverage	1871 to present
Temporal resolution	Monthly
File format	NetCDF
Update frequency	Monthly

Table 2.2: HadISST data description from ucar.edu.

2.2 Seasonal forecasts data: SEAS5

ECMWF has been operating real-time seasonal forecast systems since 1997. Since then, the seasonal forecasting system has been updated approximately every five years. In November 2017, System 4 (SEAS4), which had been in operation since 2011, was replaced by the fifth-generation seasonal forecast system, SEAS5 (Johnson et al., 2019). Similar to other seasonal forecasting models, it provides predictions of average atmospheric, oceanic, and land surface conditions up to seven months in advance (ECMWF, 2018). SEAS5 couples the upgraded Integrated Forecasting System with the NEMO (Nucleus for European Modelling of the Ocean) ocean model and the LIM2 sea-ice model, enabling the reliable provision of seasonal climate forecasts. The NEMO component has undergone significant upgrades since SEAS4; its horizontal resolution increased from 1° to 0.25°, while its vertical resolution expanded from 42 to 75 layers, with a particular enhancement in the uppermost part of the ocean (Johnson et al., 2019). The increase in horizontal resolution enhances the modelling of sharp fronts and ocean transport, whereas

the higher vertical resolution improves the identification of the diurnal cycle of sea surface temperature (ECMWF, 2018). Johnson et al. (2019) demonstrated that these improvements in ocean model resolution significantly contributed to the reduction of the cold tongue bias, a systematic error in which the model's prediction for SST in the equatorial Pacific was anomalously colder than observed reality. According to the same studies, mitigating this bias leads to improved predictive skill for the El Niño-Southern Oscillation (ENSO), a phenomenon that strongly influences the global climate (McPhaden et al., 2006).

Additionally, the atmospheric horizontal resolution received a notable upgrade from SEAS4, increasing from 80 km to 36 km (ECMWF, 2018). Another significant innovation in SEAS5 is the implementation of the interactive LIM2 sea-ice model; whereas SEAS4 treated sea ice as a static boundary condition based on historical statistics, SEAS5 is capable of simulating sea-ice dynamics in response to changes in atmospheric or oceanic conditions (ECMWF, 2018).

SEAS5 consists of a 51-member ensemble initialized on the first day of each month and integrated over a 7-month period (Johnson et al., 2019). Each member is executed starting from slightly perturbed initial conditions in order to reduce chaotic noise; this makes the final output, which is the average of all 51 members known as the ensemble mean, substantially more robust (Molteni et al., 1996). Furthermore, 15 of the 51 ensemble members are integrated for an extended total of 13 months exclusively in February, May, August, and November, with the specific aim of detecting the long-term evolution of ENSO (Johnson et al., 2019).

Finally, hindcasts play a fundamental role in model validation and bias detection (Stockdale, 2021). They consist of retrospective forecasts generated for past years that are subsequently compared against historical observational records. In other words, 25 of the 51 members of the model are run for each month throughout the 1981–2016 historical period. The comparison between these hindcasts and the observational data from the corresponding years can highlight systematic biases within the model and rigorously verify its overall accuracy (Stockdale, 2021). However, it is important to note that while the operational forecasts starting in 2017 are initialized using real-time ECMWF Operational Analyses, the hindcasts (1981-2016) are initialized using historical atmospheric and oceanic reanalyses, specifically ERA-Interim.

To mitigate excessive computational costs, only 25 of the 51 ensemble members are run for the hindcast dataset; nevertheless, this represents an increase compared to the 15 members used in SEAS4, thereby making the SEAS5 hindcasts significantly more reliable (Johnson et al., 2019). Indeed, SEAS5 outputs for the 1981–2016 period (hindcasts) are computed using a reduced set of 25 members, while from 2017 onwards (forecasts), the full 51-member ensemble is involved.

In the context of seasonal forecasting, the lead time is the temporal interval between the model initialization date (i.e. the first day of every month for SEAS5), and the validity period of the target forecast (Johnson et al., 2019). For instance, if the model is initialized on May 1st, a prediction targeting the total precipitation for the month of August corresponds to a lead time of three months. It is well established that forecast uncertainty inherently increases with lead time; as the simulation progresses further away from the initial conditions, the chaotic internal variability of the atmosphere becomes predominant, ultimately limiting the predictability of the climate system (Slingo & Palmer, 2011). Consequently, the predictive skill of the SEAS5 system progressively declines as the lead time extends (Johnson et al., 2019; Cerato et al., 2025).

For the purpose of this analysis, all the forecasts regarding summers 2003 and 2015 were evaluated using 25 members, as they belong to the hindcast dataset. In contrast, the analysis of the 2018 and 2022 events was performed using the full operational ensemble of 51 members. Furthermore, all the variables considered for this study were drawn from forecasts initialized on the 1st of May to accurately capture the target summer season minimizing the lead time and the related uncertainties. Before conducting any analysis, each variable from both datasets was geographically subset according to the established domain of study, which is defined between longitudes 25°W and 35°E, and latitudes 30°N and 75°N.

It should be noted that the northern part of the African continent will only be visualized in the anomaly maps to observe the climatic conditions of the Mediterranean region in its entirety; however, it will be excluded from all statistical calculations to strictly limit the quantitative analysis to the European continent. Conversely, MSLP will be displayed over an extended spatial domain—spanning between longitudes 45°W and 35°E, and latitudes 20°N and 90°N—in order to adequately capture the Summer North Atlantic Oscillation (SNAO) and the pressure

dynamics above the polar region. Finally, SST is visualized across the entire globe, as even distant oceanic circulation patterns can exert a significant influence on the European climate through large-scale atmospheric teleconnections. Table 2.3 below summarizes the characteristics of the SEAS5 dataset, while Table 2.4 details all the variables used in this analysis.

SEAS5	
Data type	Gridded
Projection	Regular latitude-longitude grid
Horizontal coverage	Global
Horizontal resolution	**Atmosphere:** 0.32°× 0.32° (∼36 km) **Ocean:** 0.25°× 0.25° (∼28 km) *(Note: Data often aggregated to 1°× 1° for distribution)*
Vertical resolution	**Atmosphere:** 91 levels (up to 80 km) **Ocean:** 75 levels
Temporal coverage	**Hindcasts:** 1981 to 2016 **Forecasts:** 2017 to Present (up to +7 months ahead)
Temporal resolution	From 6-hourly to daily
File format	NetCDF
Update frequency	Monthly

Table 2.3: SEAS5 Data description from Climate Data Store (CDS) Copernicus.eu.

Variable name	Units	Dataset	Description
Volumetric soil water layer 1 (soil moisture)	m^3m^{-3}	ERA5, SEAS5	Volume of water per m^3 of soil layer 1 (0–7 cm, the surface is at 0 cm).
2m air temperature (t2m)	K	ERA5, SEAS5	Temperature of air at 2m above the surface of land, sea or inland waters.
Maximum 2m temperature since previous post-processing (mx2t)	K	ERA5	Highest temperature of air at 2m above the surface of land, sea or inland waters since the parameter was last archived.
Minimum 2m temperature since previous post-processing (mn2t)	K	ERA5	Lowest temperature of air at 2m above the surface of land, sea or inland waters since the parameter was last archived.
Maximum daily 2m temperature (mx2t24)	K	SEAS5	Highest daily temperature of air at 2m above the surface of land, sea or inland water.
Minimum daily 2m temperature (mn2t24)	K	SEAS5	Lowest daily temperature of air at 2m above the surface of land, sea or inland waters.
Total precipitation (tp)	m	ERA5, SEAS5	Accumulated liquid and frozen water, comprising rain and snow, that falls to the Earth's surface.
Mean sea level pressure (MSLP)	Pa	ERA5, SEAS5	Pressure of the atmosphere at the surface of the Earth, adjusted to the height of mean sea level.
Sea Surface Temperature (SST)	K	HadiSST, SEAS5	Temperature of sea water near the surface.

Table 2.4: Units, dataset and description of the variables involved in this analysis.

Chapter 3

Methodology

This chapter describes the calculation of the Standardised Water Balance Anomaly (SWBA), the Brier Score, the climatological anomalies, and the SNAO index, other than a step-by-step description of the Significance test.

3.1 Water balance

We define the water balance as the difference between the amount of rainfall (P) in mm occurred in a given period of time and the potential evapotranspiration (PET) in mm in the same time and area.

The use of potential evapotranspiration rather than actual evapotranspiration (ET_α) is due to its only dependency on atmospheric conditions (air temperature, solar radiation) rather than soil properties. Unlike ET_α which rely on the actual water availability of the soil, the PET is the absolute measure of the "atmospheric demand"; it is a climatic parameter that can be estimated from weather data (Allen et al., 1998).

The summer water balance at every grid point of the study area was computed by aggregating the monthly water balance (P-PET) over the JJA season, using both ERA5 reanalysis and SEAS5 seasonal forecast datasets. The PET was computed through the Hargreaves formula, officially used in the SPEI computation (Beguería et al., 2014). The method gives an estimation of PET starting from the daily maximum and the minimum air temperature, and the latitude. The formula is the

following:

$$\mathrm{PET} = 0.0023 \cdot R_\alpha \cdot (T_{\mathrm{mean}} + 17.8) \cdot \sqrt{T_{\mathrm{max}} - T_{\mathrm{min}}} \tag{3.1}$$

Where $T_{\mathrm{mean}} = \dfrac{T_{\mathrm{max}} + T_{\mathrm{min}}}{2}$ and $R_\alpha\,[\mathrm{mm\,day^{-1}}]$ is the extraterrestrial radiation, a latitude-dependant variable which strongly influences the PET (Allen et al., 1998). Overall, water balance is widely regarded in hydro-climatology as a robust proxy for water availability, environmental health and drought detection (Thornthwaite, 1948; Vicente-Serrano et al., 2010).

3.2 Standardized Water Balance Anomaly

For this analysis, we defined a numerical index, namely the Standardized Water Balance Anomaly (SWBA), to assess the occurrence of a drought event, starting from atmospheric variables. The Index is computed following a step-by-step process two times, once using ERA5 Reanalysis data and the other using SEAS5 forecast data.

Before calculating climatological statistics (mean and standard deviation) I performed a linear detrending of the data. The trend must be removed to isolate interannual climate variability from long-term trend due to global warming. The linear detrending was applied to the seasonal JJA water balance time series for both ERA5 reanalysis and the model ensemble mean, and it consisted in a linear regression over the entire period [1993, 2016]. For SEAS5, the linear trend was calculated from the ensemble mean. Subsequently, to compute the predicted SWBA for each distinct ensemble member, the same ensemble-mean trend was subtracted from each member's respective water balance time series.

For each grid point (i, j) corresponding to a specific latitude and longitude, the seasonal Water Balance time series $X_{i,j}(t)$ was detrended using the following procedure: at first, the linear trend was estimated via ordinary least squares regression over the period $t \in [1993, 2016]$:

$$\hat{T}_{i,j}(t) = \hat{\alpha}_{i,j} + \hat{\beta}_{i,j} \cdot t \tag{3.2}$$

Later, the detrended anomaly $X'_{i,j}(t)$ was calculated by subtracting the trend component from the original series and adding back the local long-term mean $\overline{X}_{i,j}$:

$$X'_{i,j}(t) = X_{i,j}(t) - (\hat{\alpha}_{i,j} + \hat{\beta}_{i,j} \cdot t) + \overline{X}_{i,j} \tag{3.3}$$

Where:

- i, j represent the spatial coordinates (latitude and longitude);
- t is the time step (year);
- $X_{i,j}(t)$ is the summer water balance at location (i, j) and time t before detrending;
- $\hat{\alpha}_{i,j}$ and $\hat{\beta}_{i,j}$ are, respectively, the regression intercept and slope coefficients calculated for each grid point;
- $\overline{X}_{i,j}$ is the climatological mean at location (i, j) within [1993, 2016].

The dependency on location of each factor is due to the spatial variability of the trend; it enables the method to account for different rates of warming or drying in different regions of the domain. The statistical parameters for standardization were derived from a fixed reference period spanning from 1993 to 2016, in order to be consistent with the standard fixed hindcast period defined by the Copernicus Climate Change Service (C3S) for seasonal forecasts (Stockdale, 2021).

Both the mean $\overline{(P - PET)}_{1993,2016}$ and the standard deviation $\sigma_{1993,2016}$ were calculated using only the JJA detrended data within this 23 years-window. Finally, the SWBA can be computed as a Z-score for each grid point of the map using the following formula:

$$\text{SWBA}_{i,j} = \frac{(P - \text{PET})_{i,j,y} - \overline{(P - \text{PET})}_{1993,2016,i,j}}{\sigma_{1993,2016,i,j}} \tag{3.4}$$

Where y stays for the specific year case of study (2003, 2015, 2018, 2022) and (i, j) refer to the specific location. In this way, each grid point will be associated to its SWBA value which will enable drought detection and direct comparison even between pixels belonging to locations with two completely different climate types.

In addition to displaying and comparing the absolute magnitude and effect of droughts in Europe during these specific summers, the aim of the index is to establish unequivocally when a drought can be defined as such. In this thesis, a

threshold of -1.0 was established, stating that a drought can be defined as such when the detrended SWBA is less than or equal to -1. This threshold was chosen knowing that SWBA can be compared to SPEI index (see Section 1.1) and, although it was originally defined by Vicente-Serrano et al. (2010), its classification of drought severity adopts the standard probability thresholds established for the SPI by McKee et al. (1993), where a drought event is formally defined when the index values fall below -1.0 (WMO, 2016).

3.3 Brier Score

As already stated, one of the aims of this study is to assess the SEAS5 prediction accuracy of the droughts occurred in Europe during summer 2003, 2015, 2018, and 2022. The Brier Score (BS) serves as a metric of verification in the field of seasonal forecasting and meteorology, where predictions are expressed in probabilities of occurrence. Once the threshold for defining a drought event has been established, it is possible to assign the value of 1 to each grid point where drought occurred and the value of 0 where it did not occur, according to ERA5 data. This represents the O value mentioned below in Eq. 3.5 and 3.6.

Starting from there, it was then possible to calculate the fraction of SEAS5 model members that predicted $SWBA \leq -1.0$ and thus the probability ($p_{i,j}$) that the model would foresee the drought event for each location (i, j) of the study area. The Brier Score corresponds to the squared difference between the forecast probabilities and the binary observations at any location (i, j) (Wilks et al., 2011). At each grid point, the BS was computed using the following formula:

$$\mathrm{BS}_{i,j} = (p_{i,j} - O_{i,j})^2 \tag{3.5}$$

Since $p_{i,j}$ is a probability, $0 \leq p_{i,j} \leq 1$. $O_{i,j}$ can only assume the value of 1 or 0. Therefore, $0 \leq BS \leq 1$. The lower the BS, the higher the accuracy of the forecast (Wilks et al., 2011). In this study, the events to predict are summer droughts. First, the areas in which the droughts occurred according to ERA5 are identified using -1 as a threshold for the SWBA. Each grid point was then linked to the value of 1 if $SWBA \leq -1.0$ (the drought occurred) or to the value of 0 if SWBA > -1.0 (the

drought did not occur). For each grid point, the number of members (out of 25 for 2003 and 2015, and out of 51 for 2018 and 2022) which predicted a $SWBA \leq -1.0$ was computed: the fraction of this number over the total number of members is the probability of drought occurrence. The area-weighted average BS was then computed considering only the $p_{i,j}$ values of the grid points belonging to the domain where the drought event occurred according to ERA5, using Eq. 3.6:

$$\mathrm{BS} = \frac{1}{n}\sum_{k=1}^{n}(p_k - O_k)^2 \tag{3.6}$$

Where k refers to the specific grid point. All the grid points where no droughts occurred have been excluded by the statistical computations because the aim is to evaluate the SEAS5 seasonal forecast accuracy in specifically predicting the drought events. If grid points where no drought occurred were also considered, the general accuracy of the model in predicting the overall summer water balance would be assessed, not just critical water stress conditions.

3.4 Climatological Anomalies

Later in the analysis, the climatological anomalies of Soil moisture, 2m air temperature, total precipitation, mean sea level pressure, and sea surface temperature were computed for the four summers under observation (2003, 2015, 2018, 2022) in order to assess the variations of the main atmospheric and oceanic variables compared with the average climate. The concept of "average climate" refers to the mean JJA climatology of the reference period [1993,2016]. This time span is coherent with the standard fixed hindcast period defined by the C3S for seasonal forecasts (Stockdale, 2021). The choice of 1993 as the starting year is driven by the significant improvement in ocean observational data quality, specifically the availability of high-precision satellite altimetry and enhanced tropical mooring arrays, which are critical for the accurate initialization of the coupled ocean-atmosphere system in SEAS5 (Johnson et al., 2019). Furthermore, using recent years as a standard reference, avoids the biases given by the long-term trend of climate change. The anomalies are computed using both ERA5 Reanalysis (HadiSST for SST), and SEAS5 seasonal forecast data for all the variables just mentioned. The logic behind

the computation of the anomaly value for each grid point relies on the following formula:

$$\text{Anomaly}_{\text{JJA}} = X_{\text{JJA},y} - X_{\text{JJA},[1993,2016]} \tag{3.7}$$

In other words, the final anomaly value displayed refers to the difference between the variable mean during the summer under study (y = 2003, 2015, 2018, 2022), and the same variable mean computed over all the JJA seasons of the climatology reference period [1993,2016]. The only exception was done for Soil moisture, which anomalies have been computed for the month of May.

The anomalies computed for the seasonal forecasts have been averaged for the ensemble mean, considering the mean of the variable $\langle X^{e}_{\text{JJA},y} \rangle$ over all the 51 members (or 25 for the hindcast). Positive anomalies are linked with an increase of the variable during the target summer, while negative anomalies correspond to a drop of the same variable, in comparison with the mean value of the standard reference period, which corresponds to what it is "expected" to measure. Anomalies value close to zero are related to the absence of exceptional events.

3.5 Significance Test

Once the summer anomalies were calculated, it was possible to observe the behaviour of each member within the SEAS5 seasonal forecast for the selected summers. This process enabled the identification of the eight driest and wettest members of the model's ensemble. The selection of these sub-ensembles was strictly based on the water balance predicted by each individual member.

A drought mask was initially defined using the ERA5 reanalysis data by selecting only the grid points where the SWBA fell below -1.0, thereby isolating all the locations where a drought effectively occurred. Subsequently, all SEAS5 members were ranked according to their spatially averaged water balance specifically within this predefined mask. The eight members predicting the lowest water balance were selected and classified as the "driest" members, while the eight members predicting the highest water balance were categorized as the "wettest" members. Following this categorization, the composite anomalies for each summer were computed by calculating the average anomalies for both the eight driest and the eight wettest members.

Finally, to verify whether the atmospheric and oceanic anomalies identified within the selected sub-ensembles represent a robust physical signal rather than belonging to internal model variability, a non-parametric statistical significance test was applied across each grid point for t2m, tp, MSLP, and SST. To do so, we test whether the composite mean of the selected $k = 8$ members differ significantly from a random selection of 8 members drawn from the same ensemble pool. For a given year and variable, let N be the total number of available ensemble members ($N = 51$ for the 2018 and 2022 forecast and $N = 25$ for the 2003 and 2015 hindcasts). Let S_{obs} be the set of indices corresponding to the $k = 8$ members selected based on the Water Balance ranking (either "driest" or "wettest"). The observed composite mean $\overline{X}_{obs}$ for a specific grid point (i, j) is calculated as:

$$\overline{X}_{\text{obs}}(i,j) = \frac{1}{k} \sum_{m \in S_{\text{obs}}} X_m(i,j) \tag{3.8}$$

Where $X_m\,(i, j)$ represents the value of the anomaly of member m at that location. To estimate the probability of obtaining such a signal by chance (the Null Hypothesis

H_0), an empirical reference distribution was constructed by performing 1000 different iterations with 8 members casually drawn. The random composite mean $\overline{X}_{rand}^{(b)}$ was computed for each iteration:

$$\overline{X}_{\text{rand}}^{(b)}(i,j) = \frac{1}{k} \sum_{m \in S_{\text{rand}}^{(b)}} X_m(i,j) \tag{3.9}$$

This process gives as outcome the distribution of 1000 potential outcomes representing the internal variability of the model for that specific year. The statistical significance was determined using a two-tailed test with a confidence level of 95% ($\alpha = 0.05$). It has been tested whether the observed mean $\overline{X}_{obs}$ fell into the extreme tails of the generated distribution. Two empirical p-values were calculated for each grid point by counting the occurrences where the random means exceeded or fell short of the observed mean:

$$p_{\text{lower}} = \frac{1}{1000} \sum_{b=1}^{1000} \mathbb{I}\left(\overline{X}_{\text{rand}}^{(b)} < \overline{X}_{\text{obs}}\right) \tag{3.10}$$

$$p_{\text{upper}} = \frac{1}{1000} \sum_{b=1}^{1000} \mathbb{I}\left(\overline{X}_{\text{rand}}^{(b)} > \overline{X}_{\text{obs}}\right) \tag{3.11}$$

Where $\mathbb{I}$ is the indicator function (equal to 1 if true, 0 otherwise). A grid point is defined statistically significant (rejecting H_0) if the observed mean fell within the lowest 2.5% or the highest 2.5% of the random distribution:

$$\text{Significant}_{i,j} = \begin{cases} 1 & \text{if } p_{\text{lower}} < 0.025 \text{ or } p_{\text{upper}} < 0.025 \\ 0 & \text{otherwise} \end{cases} \tag{3.12}$$

With $\frac{\alpha}{2} = 0.025$. This strict threshold ensures that the anomalies in the "driest" and "wettest" maps represent anomalies that are exceptionally rare compared to the ensemble's internal noise.

3.6 SNAO Index

The variability of the North Atlantic pressure field has been examined to better understand the large-scale atmospheric drivers of the analysed drought events. The North Atlantic Oscillation (NAO) is the dominant mode of atmospheric variability in the Northern Hemisphere characterized by a pressure dipole between the Azores High and the Icelandic Low (Hurrell, 1995), but its structure changes significantly between winter and summer seasons (Folland et al., 2009).

As demonstrated by Folland et al. (2009), the canonical winter NAO pattern undergoes a northward and eastward shift during summer. This seasonal migration would be caused by the contraction of the polar vortex and the northward displacement of the Atlantic jet stream. Consequently, the centres of action responsible for steering storm tracks across Europe shift location: the Subtropical High migrates from the Azores to the British Isles and southern Scandinavia, while the Subpolar Low migrates from Iceland to southern Greenland. This distinct summer pattern is termed the Summer North Atlantic Oscillation (SNAO, Folland et al., 2009). A positive phase of the SNAO is characterized by strong anticyclonic blocking over the UK and Northern Europe, leading to warm, dry conditions in these regions and wet conditions over Greenland and Southern Europe. Conversely, a negative phase is associated with lower pressure over the UK and increased zonal flow, bringing precipitation to Northern Europe (Folland et al., 2009).

While Folland et al. (2009) originally defined the SNAO as the leading Empirical Orthogonal Function (EOF) of extratropical North Atlantic pressure, they demonstrated that a station-based index derived from the EOF's centres of action provides a robust proxy for the phenomenon. In this study, the SNAO index is calculated using a point-based difference method applied to MSLP fields from both ERA5 reanalysis and SEAS5 seasonal model. To capture the summer-specific dynamics, the coordinates identified by Folland et al. (2009) have been utilized:

- **Northern Node**: Southern Greenland ($65°\text{N}, 40°\text{W}$);
- **Southern Node**: Southern UK ($50°\text{N}, 5°\text{W}$).

This differs from the standard NAO index which typically uses Iceland and the Azores as the poles, ensuring that the index captures the right atmospheric blocking

pattern for the JJA season. Furthermore, the strong negative correlation found by Folland et al. (2009) between the SNAO index and the JJA precipitation over United Kingdom and Northern Europe confirms the SNAO as physically appropriate metric for analysing summer drought dynamics across Europe.

The calculation of the SNAO index was performed using Python following a standardized procedure for May and the JJA season. The index was computed using both the MSLP observational data from ERA5 and the seasonal forecast data from the SEAS5 model. With regard to the latter, the SNAO index was computed three different times: using the ensemble mean and the average of the 8 "driest" and the 8 "wettest" members, in order to catch whether there are any correlations between a more accurate forecast and a particular SNAO phase. The generic formula for the station-based NAO index and perfectly applicable also for the SNAO is the following (Hurrell, 1995):

$$\mathrm{SNAO}_y = \left(\frac{P_{\mathrm{South},y} - \mu_{\mathrm{South}}}{\sigma_{\mathrm{South}}}\right) - \left(\frac{P_{\mathrm{North},y} - \mu_{\mathrm{North}}}{\sigma_{\mathrm{North}}}\right) \tag{3.13}$$

Where P_y is the JJA (or May) MSLP for year y, μ is the long-term climatological mean computed for the 23-years reference period [1993, 2016], and σ is the climatological standard deviation for the same period [1993, 2016]. Two distinct approaches to calculating the standard deviation σ have been applied to ERA5 and SEAS5 indices, in order to ensure a physically meaningful comparison between the single deterministic reality of ERA5 and the probabilistic ensemble of the seasonal model. For the observational data, the mean μ and the standard deviation σ were calculated based on the time series of the reference period [1993, 2016], representing the natural interannual variability of the observed atmosphere. Regarding the SEAS5 dataset, the standardization was performed using the standard deviation of the total ensemble population (all members over the [1993, 2016] period) rather than the standard deviation of the ensemble mean over the same period. This ensures that the magnitude of anomalies in individual members (e.g., 8 driest/8 wettest members) is directly comparable to the magnitude of observed anomalies in ERA5, treating both as single realizations of a chaotic system.

Chapter 4

Results

Throughout this section, all results derived from the various analyses conducted using the methodologies examined in Chapter 3 will be presented and investigated.

4.1 Water Balance and Brier Score Time Series

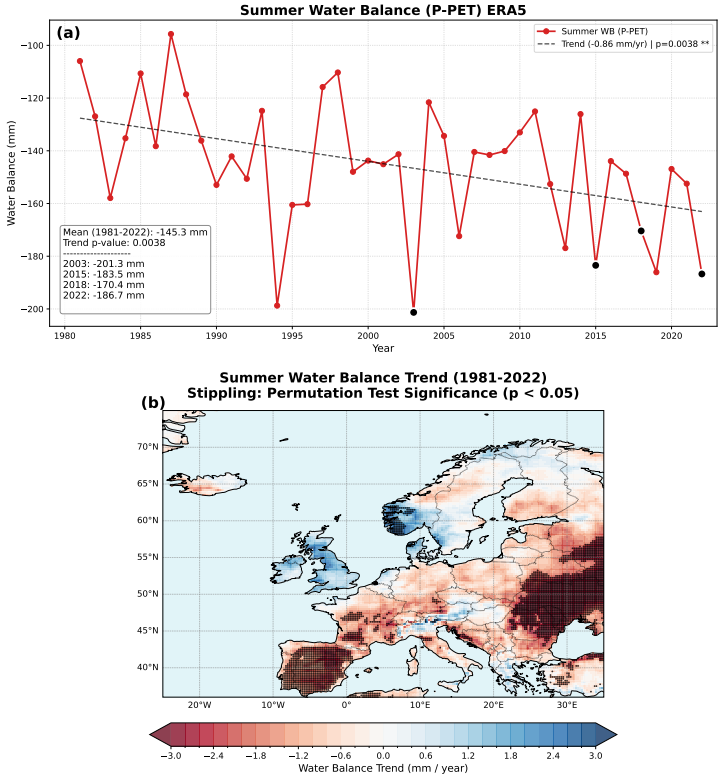

Figure 4.1: (a)Interannual variability of the accumulated European Summer Water Balance derived from ERA5 reanalysis [1981,2022]. Text box displays the mean of the accumulated European Summer Water Balance of the entire period [1981,2022], the specific values for the four summers under study and the p-value of the trend, which shows great significance of the observed trend (**, p-value $<$ 0.01).(b)Spatial distribution of the accumulated Summer Water Balance trend based on ERA5 reanalysis calculated over the period [1981,2022]. Stippling indicates statistical significance at the 95% level (p value $<$ 0.05).

The graph in Fig. 4.1a shows the evolution of the summer water balance in Europe (between longitudes 25°W and 35°E, and latitudes 30°N and 75°N) over the past 40 years, spanning from 1981 to 2022. Each year is associated with the average water balance value recorded across Europe, aggregated over the JJA season. The calculations were restricted to European terrestrial grid points, masking out the oceans and the African continent.

The water balance in question is the measure of the difference between the amount of precipitation that fell during the summer months and the amount of water that evaporated from the soil over the same period (P-PET). The difference between precipitation (P) and potential evapotranspiration (PET) quantifies the net atmospheric moisture surplus or deficit available to the hydrological system (Vicente-Serrano et al., 2010). Positive values of the water balance indicate a moisture surplus, whereas negative values imply that the atmospheric evaporative demand exceeds the available precipitation, thereby causing a water deficit in the area (Vicente-Serrano et al., 2010). P-PET was calculated as the total seasonal accumulation (in mm) over the JJA period. Consequently, the linear trend represents the interannual change of this total seasonal volume.

Overall, the graph illustrates a substantial decrease in the observed summer water balance. In general, negative water balance values ($P - PET < 0$) are to be expected during the European summer, particularly in the Mediterranean region, which represents the seasonal peak of atmospheric evaporative demand (Lionello et al., 2006); however, studies such as those by Stagge et al. (2017) and Spinoni et al. (2018) highlight that this seasonal deficit is progressively deepening. The negative trend observed in this analysis, (-0.86 mm/year, statistically significant according to a permutation test) (Fig. 4.1a),is consistent with the findings of Stagge et al. (2017) and Christidis et al. (2021). These studies confirm a widespread reduction in water availability across Europe, primarily driven by a rising evaporative demand (PET), ultimately leading to a progressive drying of the European summer climate. Furthermore, Stagge et al. (2017) highlight the primary role that the temperature increase induced by global warming plays, when compared to precipitation trends alone, in the progressive worsening of water availability in Europe.

The summer water balance trend was then computed for each grid point across Europe. Stippling in Fig. 4.1b indicates statistical significance at the 95% level (where p value < 0.05). The resulting map (Fig. 4.1b) clearly illustrates that over the last 40 years, the water balance has experienced a decreasing trend across most of the continent. However, there are evident spatial differences: the Mediterranean region (especially the Iberian Peninsula and France) and the easternmost part of the continent (Romania, Moldova, and western Ukraine) exhibit the strongest values, reaching significant anomalies of nearly -3 mm/year. Conversely, Scandinavia,

the British Isles, and the highest latitudes exhibit positive anomalies, even if not statistically significant. As mentioned in Section 1.2, global warming is causing an expansion of the Hadley cell, which leads to the poleward shift of subtropical high-pressure systems (Frierson et al., 2007), and may contribute to the significant trend identified here. During winter, this manifests as a significant north-eastward expansion of the Azores High, deflecting Atlantic storm tracks northward and consequently reducing the amount of precipitation in the Mediterranean region (Cresswell-Clay et al., 2022). Bladè et al. (2012) have shown that even during summer, the Azores High exhibits a growing trend to shift north-eastward, frequently relocating over the British Isles and Scandinavia. This displacement deprives the Mediterranean of the traditional temperate summer climate typically provided by the Azores High, leaving the region vulnerable to Saharan warm air intrusions, which have characterized Mediterranean summers in recent years, particularly in the Iberian Peninsula (Sousa et al., 2019). These hot, dry, continental air masses, whose effects are exacerbated by the recent amplified warming of the North African landmass, can generate severe heatwaves and drastically spike PET(Sousa et al., 2019).

Central-eastern Europe, particularly Romania, Moldova, and western Ukraine, shows the strongest significant negative values in the water balance trend (Fig. 4.1b). Ionita et al. (2017) explained that the mechanism contributing to the severity of the summer 2015 drought in those areas was a persistent blocking high-pressure system, which prevented the occurrence of precipitation and caused PET values to surge due to exceptionally high temperatures. This process is becoming a discernible tendency (as mentioned in Section 1.2), and it is expected to evolve into the climatological norm for the area (Cheval et al., 2014). Finally, the intrinsic continental climate of the region makes it even more vulnerable to such blocking high-pressure systems (Cheval et al., 2014).

Fig. 4.1b shows that the high latitudes (i.e. British Isles and Scandinavia), exhibit positive variations in the summer water balance from 1981 to 2022. Despite PET has increased in these areas due to temperature rises associated with global warming (Lindsey et al., 2020). The overall water balance has not changed much from historical baselines due to a concurrent rise in summer precipitation; this increase has been observed in the region in recent years, particularly in early summer

(June and July), and is emerging as a significant trend (Yiou and Cattiaux, 2013) especially in Southern Norway (Fig. 4.1b). Screen (2013) identified a correlation between the melting of Arctic ice and the summer jet stream, which influences the weather in northern latitudes. The article explains how Arctic sea ice loss induces a southward shift of the polar jet stream during summer, thereby increasing northern European precipitation. Generally, dry summers in the region have occurred when the jet stream is located further north (Screen, 2013).

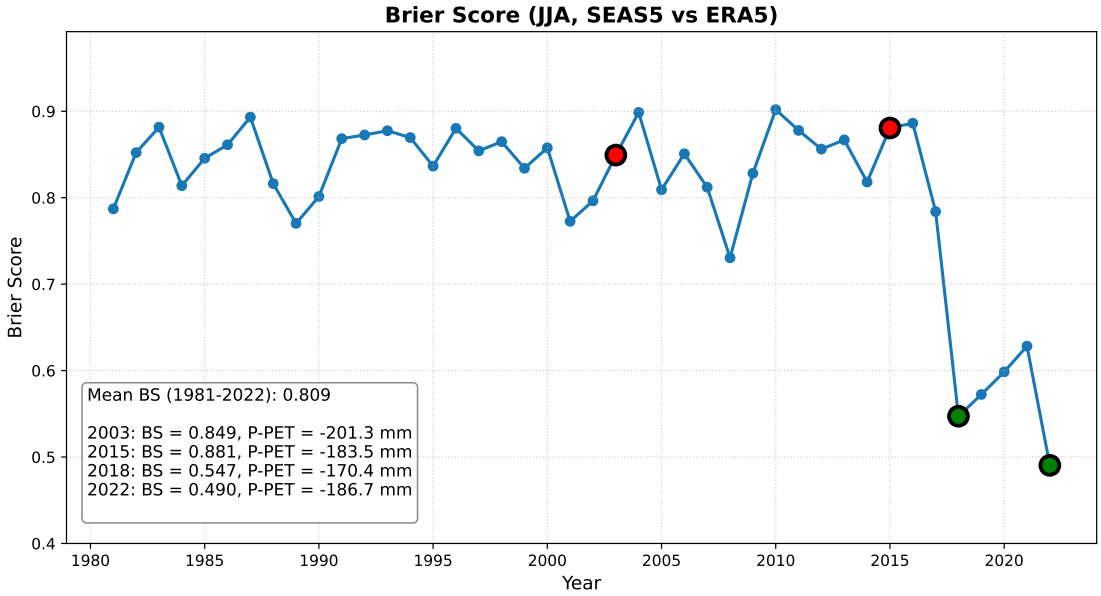

Figure 4.2: Interannual variability of the Brier Score for European summer drought prediction. The score is computed exclusively for the European grid points where drought was observed according to the ERA5 Reanalysis. Text box displays the area-weighted average Brier Score computed both for the entire period [1981,2022] and for the four summers under study taking into account only the grid points where the summer drought was recorded according to ERA5 data. Text box displays also the P-PET value related to each summer. Red dots in the time series indicate the poor-predicted summers of 2003 and 2015, while green dots indicate the well-predicted ones of 2018 and 2022.

After reviewing the historical P-PET, we evaluated the BS for droughts seasonal forecasts generated by the ECMWF seasonal model SEAS5 (Fig. 4.2). As previously discussed, the BS measures the accuracy of probabilistic forecasts (Richardson, 2001) for binary events (here, drought occurrence). A lower BS indicates a higher accuracy

of the SEAS5 model on summer SWBA prediction over Europe. Conversely, a higher value signifies that the forecast deviated significantly from the actual observed conditions (see Section 3.3). The BS time series was calculated for the 1981–2022 period, exclusively considering the grid points of the European continent that were actively affected by drought conditions. The decision to focus this analysis on the summers of 2003, 2015, 2018, and 2022 was based on the intersection of these two critical factors: the severity of the water balance deficit and the corresponding forecast accuracy as measured by the BS. All four summers exhibited strongly negative water balance values (Fig. 4.1a), indicating the occurrence of intense drought events. At the same time, these four seasons were specifically selected based on their corresponding JJA BS: the summers of 2003 and 2015 are characterized by exceptionally high BS values (0.849 and 0.881, respectively as shown in Fig. 4.2), suggesting that the SEAS5 model issued inaccurate probabilities for the drought events of those seasons. On the other hand, the summers of 2018 and 2022 demonstrate substantially lower BS values (0.547 and 0.490, respectively as shown in the text box in Fig. 4.2), indicating more accurate seasonal forecasts.

These four summers possess even unique climatological peculiarities that make them particularly compelling case studies. The summer of 2003 was exceptionally dry for its time, featuring negative water balance values comparable in magnitude to those recorded during more recent, anthropogenically amplified summers. This finding is highly significant considering that in 2003, the expected climatological baseline for the summer water balance was higher than what is expected today, owing to the progressive negative trend (see Fig. 4.1a). According to Garcia-Herrera et al. (2010), the summer of 2003 was the warmest experienced across Europe and the Mediterranean region in over 500 years. Stott et al. (2004) confirmed that anthropogenic warming had effectively doubled the likelihood of such a severe drought occurring.

The summer of 2015 is particularly interesting from a forecasting perspective because it yielded one of the highest BS values of the time series (Fig. 4.2). This indicates that SEAS5 struggled in issuing accurate probabilities for that drought event, making it an ideal diagnostic case study. Although its geographical extent was largely confined to Central and Eastern Europe, the summer drought of 2015 was considered one of the most severe in recent decades, locally surpassing even the

2003 event in terms of intensity (Ionita et al., 2017). Considering the most intensely affected areas, stretching from the Czech Republic to Ukraine, the summer of 2015 was one of the the hottest and climatologically driest summers over the 1950–2015 study period, ranking as the sixth most severe when evaluating the continent as a whole (Ionita et al., 2017).

The summer of 2018 was selected because, trailing only 2022, it represents the drought most accurately predicted by the SEAS5 model. The JJA season of 2018 was extraordinary in climatological terms for northern and central Europe, bringing severe heat and extreme drought to large parts of the continent, resulting in extensive impacts on agriculture, ecosystems, water supply, and the broader socio-economic sector (Rousi et al., 2023).

Finally, the summer of 2022 presents the lowest water balance value of the entire analysed period. At the same time, the meteorological conditions of that exceptionally dry summer were accurately anticipated by the SEAS5 model, which concurrently recorded one of its lowest BS values for the entire study period. According to the C3S (2023), during that summer, Europe experienced the highest temperatures recorded since 1500, and for a large part of the continent, it stood as the warmest year on record. The dry period was significantly prolonged by three distinct large-scale atmospheric heatwaves during the JJA season, compounded by an intense marine heatwave in the Mediterranean Sea (Trigo et al., 2025).

This thesis aims to investigate the underlying reasons dictating the varying accuracy of the ECMWF seasonal forecasts, seeking to understand whether specific climatic drivers make certain drought events more predictable than others.

4.2 SWBA and BS

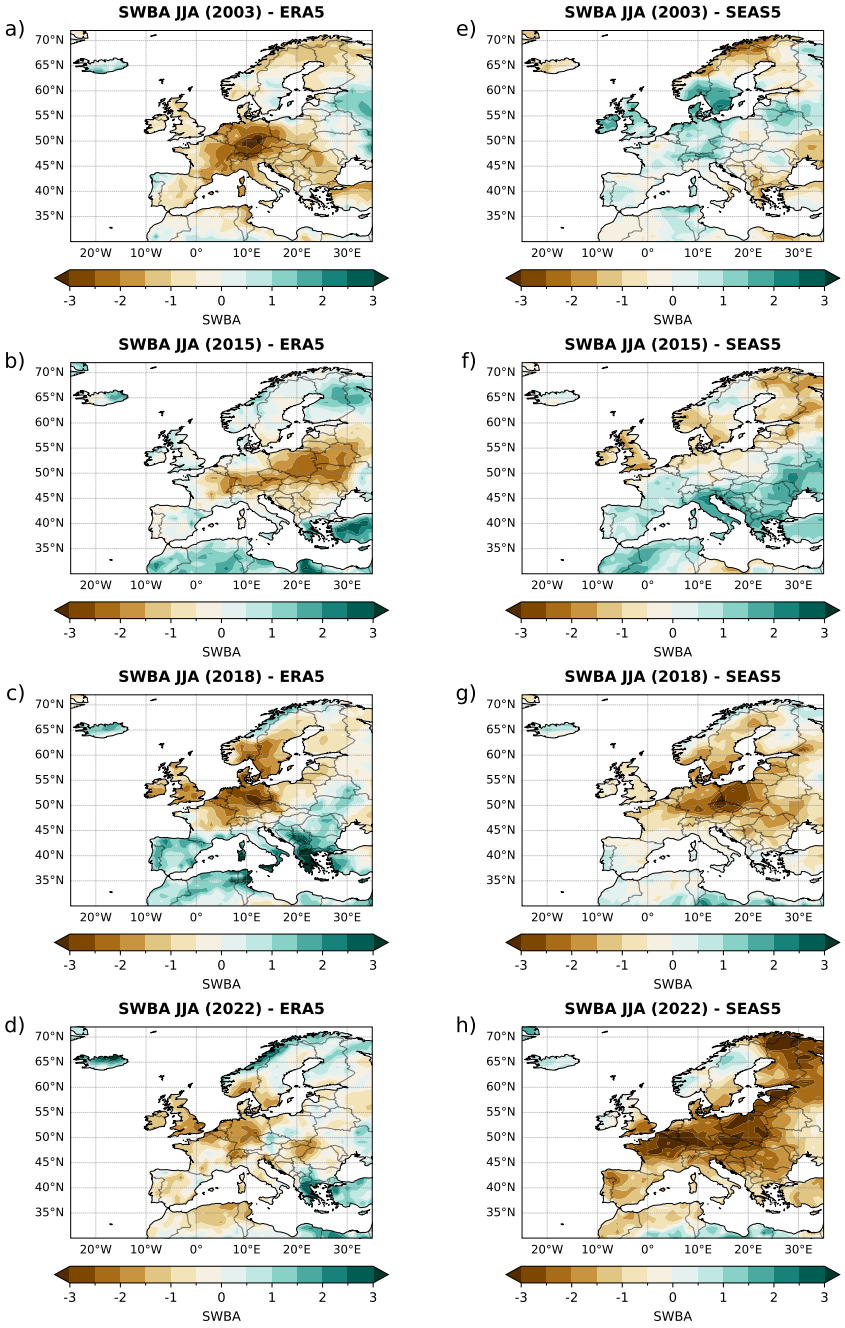

Figure 4.3: JJA Standardized Water Balance Anomaly for the target drought years relative to the 1993–2016 climatology. Left column (a–d): ERA5 reanalysis; Right column (e–h): SEAS5 ensemble mean.

The maps in Fig. 4.3 show the spatial distribution in Europe of the Standardised Water Balance Anomaly recorded in the four summers under study (JJA season). The maps to the left (Fig. 4.3a-d) refer to the SWBA computed with the Reanalysis data from ERA5, while the maps to the right (Fig. 4.3e-h) display the seasonal model's predicted value of the SWBA for each of the summers.

Fig. 4.3a shows that during summer 2003 most of the continent recorded a lower than usual water balance value, particularly the entire Mediterranean region, Central and Eastern Europe, the Balkans, but also the British Isles and the higher latitudes of Scandinavia, the latter being a particularly unique finding compared to the other three summers analysed here. During summer 2015, on the other hand, negative values were recorded more locally in Central and Eastern Europe (Fig. 4.3b). The drought of summer 2018, similar to that of 2015, remained confined to a single area, this time central-northern Europe, including the British Isles and the southernmost latitudes of the Scandinavian peninsula, which experienced extremely low water balance peaks (i.e. well below the alert threshold of -1.0, Fig. 4.3c). During the 2022 summer (Fig. 4.3d), negative SWBA was recorded across most of the continent, except for the northernmost latitudes of Scandinavia, Greece and Turkey. The latter, apart from summer 2003, experienced wetter-than-normal summers in conjunction with the drought events analysed here, coherently with the different warming rate of the area (see Section 4.1).

The maps on the right column (Fig. 4.3e-h) show the predicted value of SWBA according to the SEAS5 ensemble mean. Fig. 4.3e and Fig. 4.3f shows the ensemble mean SWBA forecast for the JJA drought of 2003 and 2015 initialized on the 1st of May. In 2003, the model predicted a wetter than usual summer (Fig. 4.3e), with significant drought conditions only in northern Scandinavia, effectively demonstrating poor forecasting accuracy. In 2015, it is noteworthy that central-eastern Europe, the area most affected by drought that summer, is the area that, together with the Alps, show the highest Water Balance forecasts on the continent (Fig. 4.3f). According to the SEAS5 ensemble mean, the area most affected by drought in 2015 would have shown an SWBA of around +3, which corresponds to a much wetter-than-normal summer. On the other hand, the 2018 and 2022 maps prove that the drought happened during those summers was already forecasted with 1 month lead. For most of the continent, both Fig. 4.3g and Fig. 4.3h show water

deficit forecast, in some cases even more severe than what happened, if compared with the maps for the same years from ERA5. Therefore, the seasonal model correctly predicted the occurrence of droughts in its ensemble mean, indicating high inter-members agreement.

Afterwards, to better localize the drought events under consideration, only the grid points associated with a SWBA value lower than -1.0 have been selected and displayed in red, both according to ERA5 (Fig. 4.4a-d) and SEAS5 datasets (Fig. 4.4e-h). The red grid points have been counted to understand the extent of both the observed and predicted drought event(Fig. 4.4).

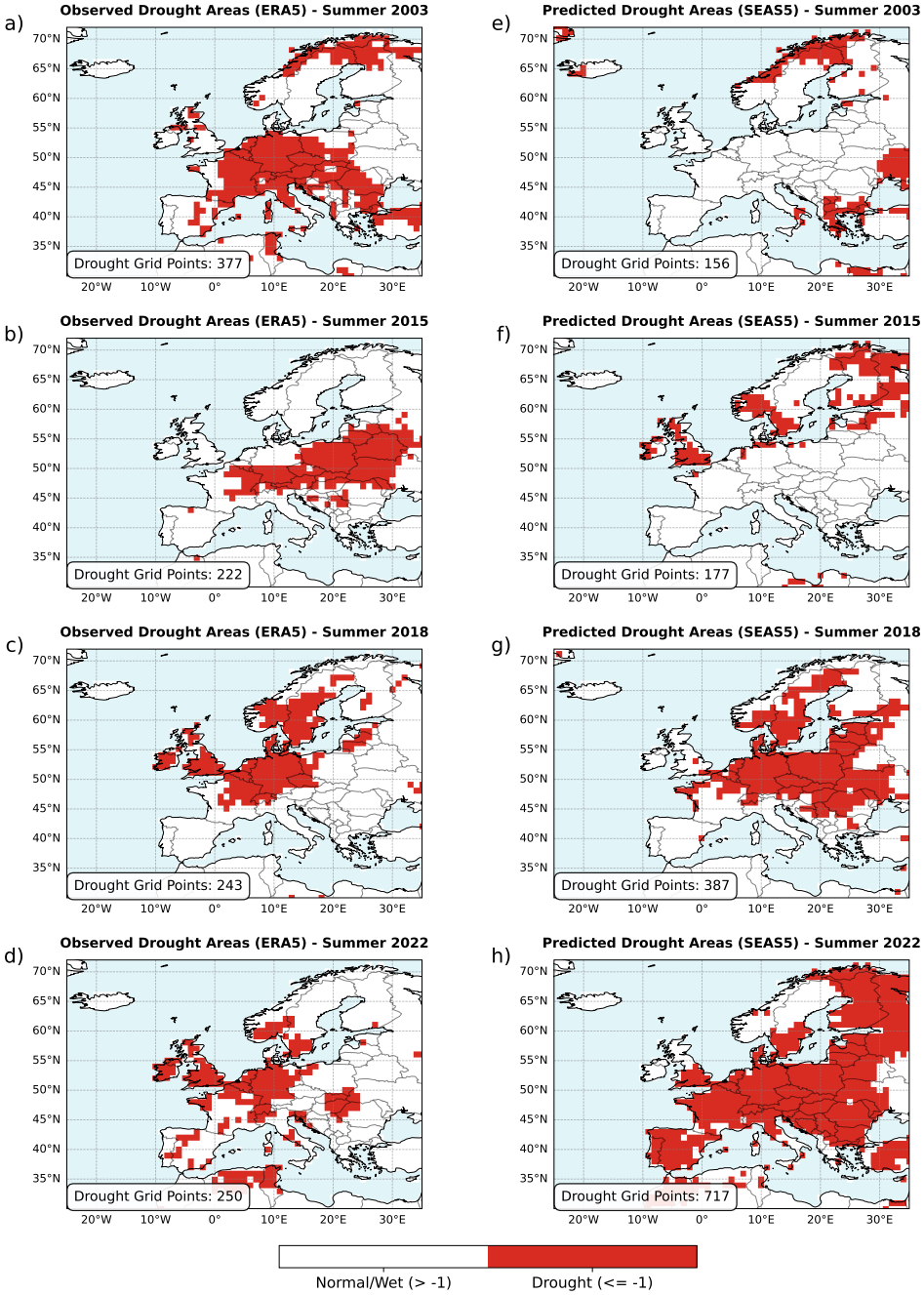

Figure 4.4: Observed (left, a-d) and predicted (right, e-h) drought areas (red pixels) for the target summers [2003, 2015, 2018, 2022]. Observed drought areas refer to ERA5 reanalysis dataset. Predicted drought areas refer to the SEAS5 ensemble mean. Text box displays the number of red grid points which are affected by drought conditions.

Among the poorly predicted summers here analysed, 2003 proved to be the worst case. Only 156 grid points were reported as being drought affected by the SEAS5 ensemble mean, whereas the actual observed were 377 (Fig. 4.4a-e). In addition, Fig. 4.4a and Fig. 4.4e demonstrate that the drought recorded in northern Scandinavia is the only one correctly identified by the model's ensemble mean, together with part of Greece. However, it failed through the rest of the continent, particularly central Europe which was the most affected area during that summer (Black et al., 2004). Dealing with summer 2015, the model ensemble mean did not foresee the dry event, which was expected to occur in only 177 grid points of the map all located in the northern part of the continent (Fig. 4.4f).

On the other hand, summer 2018 seems to be the best predicted by the model, both in terms of location and magnitude of the phenomenon (243 grid points affected by drought versus 387 predicted, Fig. 4.4c-g). In fact, drought was observed broadly in the same regions where it had been predicted, except in the British Isles and in eastern Europe, where the prediction was missed (Fig. 4.4c-g). Although it appears to be the year in which the model performed at its best, 2018 is associated with a slightly higher BS than 2022, which mathematically was recognised as the summer drought best predicted in this thesis, among the four analysed. This is due to the overestimation of the phenomenon in 2022, a summer in which the model predicted water stress across the entire continent, when the event was more limited (717 pixels reported at risk compared to 250 effectively affected, Fig. 4.4d-h). Since the BS was calculated considering only the grid points where, according to ERA5, drought occurred, the overestimation of the model made it easier the well-performance of that subset of pixels, resulting in a particularly low BS.

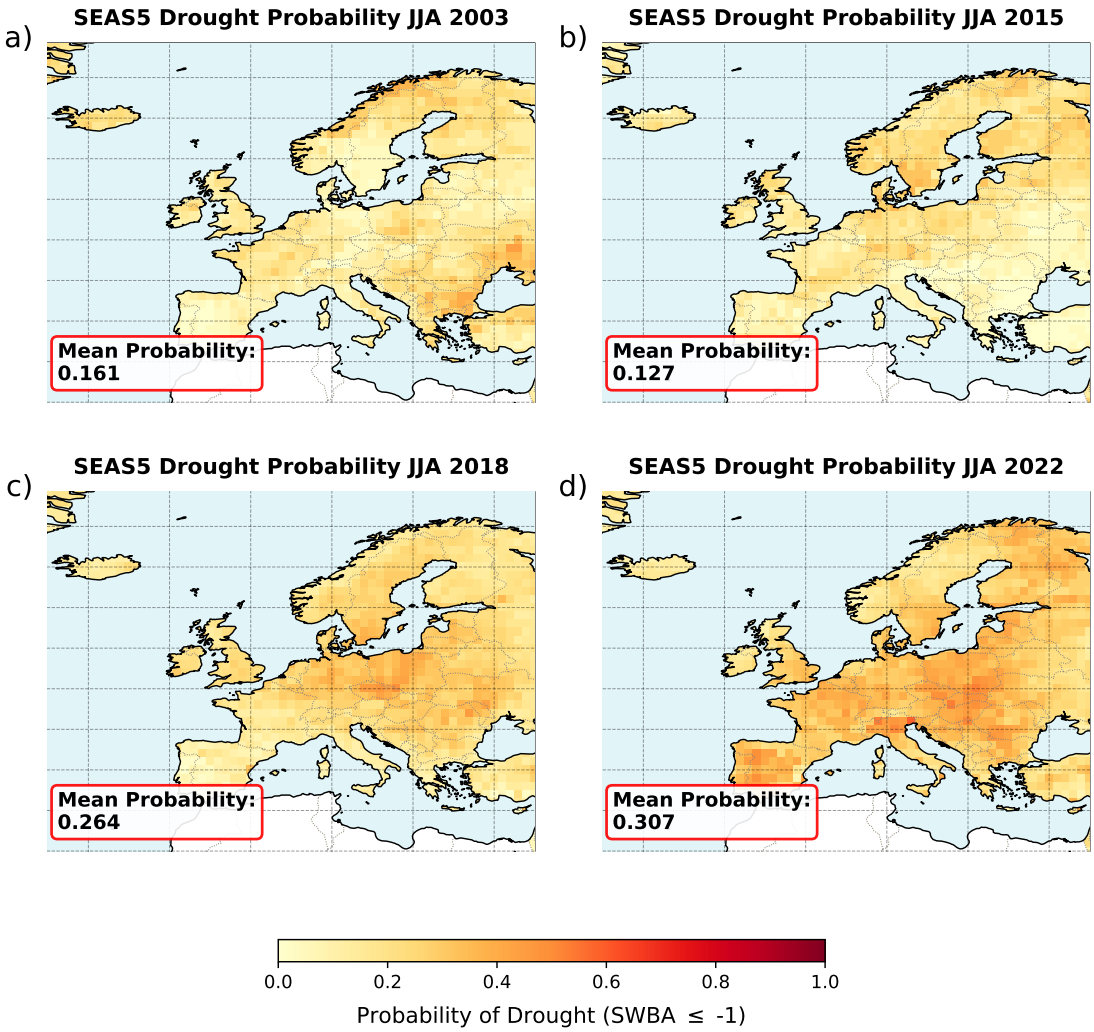

Figure 4.5: SEAS5 forecast probability of summer drought conditions for the target years. Text boxes display the mean probability computed considering all the grid points of the domain.

The average drought occurrence probability (i.e. the fraction of ensemble members predicting SWBA < -1) for the four intense droughts are displayed in Fig. 4.5. As expected, from the BS analyses, summers in which the model predicted positive or almost zero changes in water balance show lighter pixels, because only a few members predicted a drought event. The redder areas on these maps (Fig. 4.5a-b) consistently coincide with the few areas that had predicted drought in 2003 and 2015, but still remain lighter than the areas where $SWBA \leq -1.0$ was

predicted in 2018 and 2022 (Fig. 4.5c-d), as the confidence was significantly lower (lower inter-members agreement). On the other hand, the 2018 and 2022 maps (Fig. 4.5c-d) show a higher quantity of reddish pixels, reflecting the model's greater confidence in predicting the drought event for those summers.

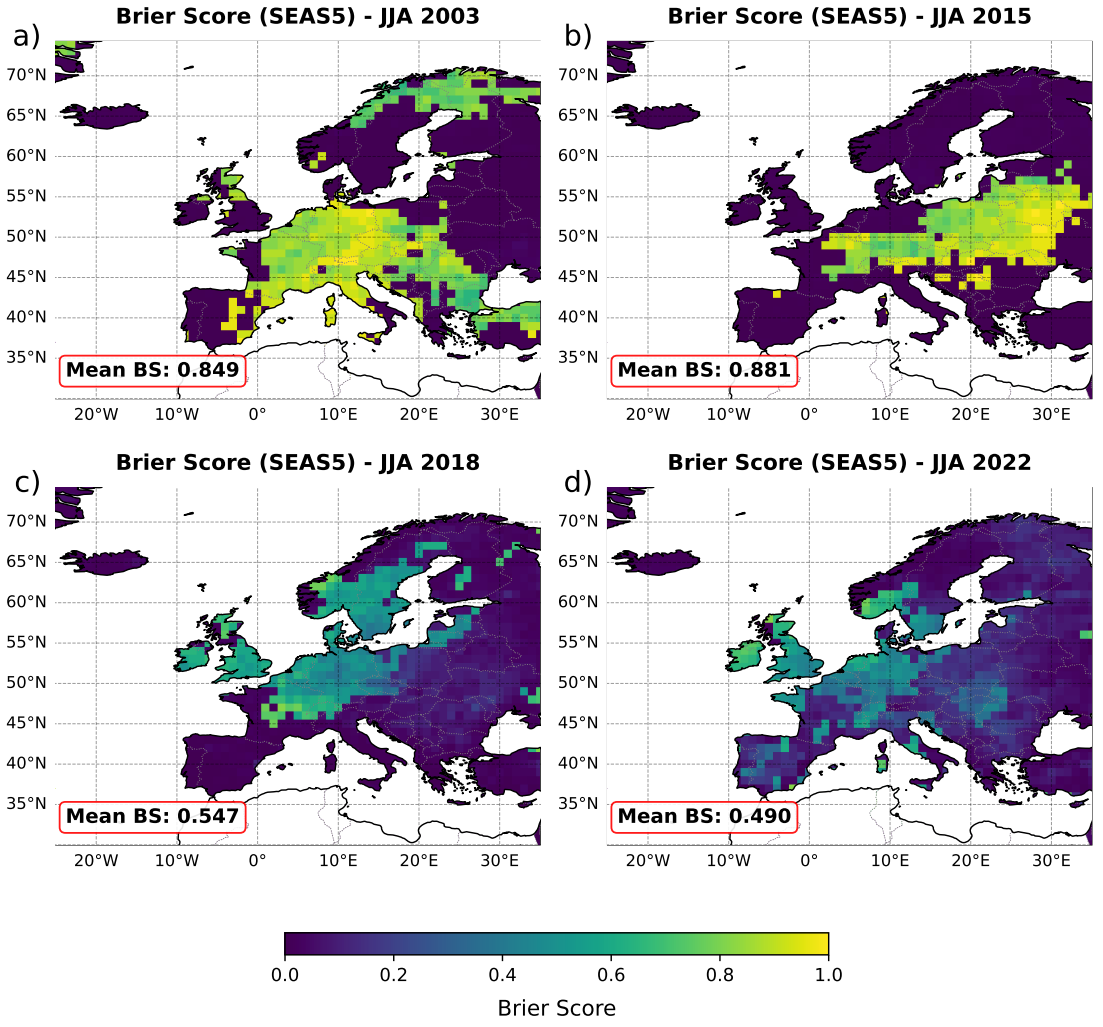

Figure 4.6: Spatial distribution of the Brier Score for SEAS5 Summer drought predictions. Text boxes display the Mean BS computed considering only the grid points of the domain where the drought occurred.

Fig. 4.6 spatially plot the BS, which refers to the accuracy of the SEAS5 model in predicting drought events. The resulted maps in Fig. 4.6 are the final

confirmation of the forecast accuracy assessment in terms of European summer droughts of the seasonal forecasting model SEAS5.

Summer 2015 was the one presenting the highest mean BS value (0.881, Fig. 4.6b), confirming it as the JJA season with the worst predicted summer drought of the four here analysed. Indeed, the majority of the pixels with the highest values (the yellowish ones) are located in areas of central and eastern Europe where the worst effects of that drought were recorded and where the model had predicted a cooler and rainier summer. The 2022 summer drought, on the other hand, is confirmed as the best predicted of the four, with the lowest average BS value (0.490, Fig. 4.6d), showing slightly higher BS values only in northern Britain and southern Scandinavia. The 2003 map (Fig. 4.6a) confirms that the summer drought was not accurately predicted in almost any of the affected areas, with high BS values across almost the entire drought zone. The peculiarity of 2003 remains the surprising extent of the event, which affected almost all of Europe and was not confidently predicted by SEAS5 in any of the different locations. The 2018 map (Fig. 4.6c), similar to that of 2022, recorded low BS values at the areas affected by summer drought, reflecting the satisfactory accuracy of the SEAS5 seasonal forecasts for that JJA season. Only France shows higher than average BS values, indicating a forecasting error in the area.

A consistent pattern observed across 2003, 2015, and 2018 maps is the prevalence of low BS values in regions where no drought occurred according to the ERA5 reanalysis. In these areas, the maps exhibit a uniform background colour (visualized as purple/dark blue), indicating a near-zero error. This phenomenon is driven by the quadratic nature of the Brier Score metric, which inherently suppresses the impact of low-probability false alarms. Mathematically, the BS for a single grid point where the observation is zero (O = 0) simplifies to the square of the forecast probability (${p_{i,j}}^2$) as follows:

$$BS_{i,j} = (p_{i,j} - O_{i,j})^2 = p_{i,j}^2 \tag{4.1}$$

For the forecasts of summers 2003, 2015, and 2018, the SEAS5 ensemble demonstrated high reliability in non-drought regions (Fig. 4.6). While the model may not have assigned a probability of exactly zero, it typically generated timid false alarms,

assigning low probabilities to the drought event. When these small probabilities are squared, the resulting error becomes negligible. The summer of 2022 presents a slight deviation from this pattern. In regions where no drought was observed, the BS values are notably higher compared to previous years. This increase is attributed to a shift in the ensemble distribution towards drier conditions, leading to overconfident false alarms. In these areas, a larger fraction of ensemble members predicted drought, raising the drought probability.

4.3 Climatological Summer Anomalies

Through this section, the resulted anomalies of soil moisture, 2m air temperature, total precipitation, mean sea level pressure and sea surface temperature for each of the four summers will be displayed and analysed to assess the climatic conditions which led to the development of such severe drought events. The analysis will compare the ERA5 anomalies with the SEAS5 predictions, both the ensemble and the 8 most ("driest") and least ("wettest") performative members mean, relative to the [1993,2016] climatology. The dots on the "driest/wettest" maps indicate the statistically significant anomalies (as explained in the Methodology section).

The aim of this comparison is to assess whether there are any significant atmospheric or oceanic patterns which drives the drought seasonal predictability. Unlike the other variables, soil moisture anomalies were calculated with respect to the month of May, to analyse soil moisture preconditioning immediately before summer. Note that there is a systematic underestimation of the anomaly magnitude by the model ensemble mean: this is a typical behaviour of the multi-member averaging process, which tends to smooth out extreme signals.

4.3.1 Soil Moisture

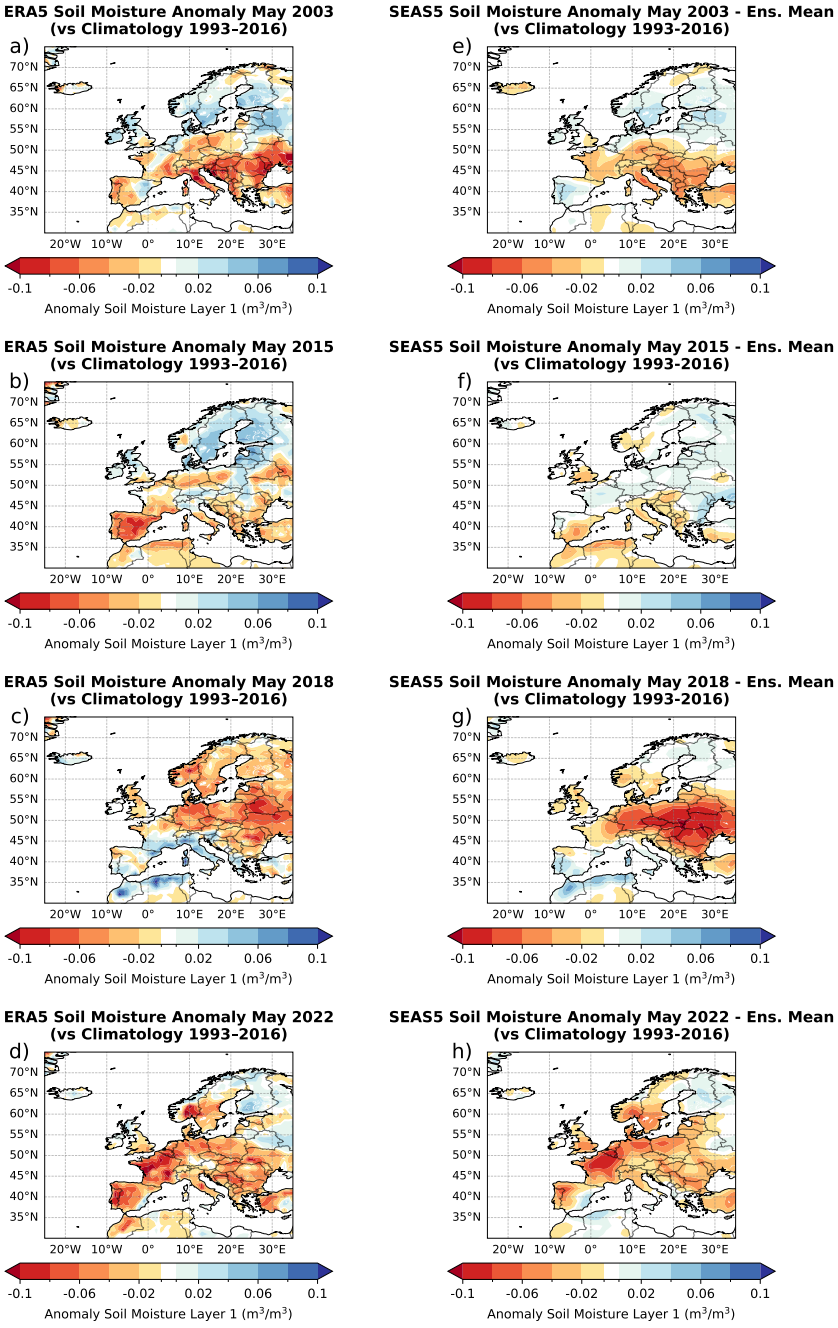

Figure 4.7: May Soil Moisture Anomalies relative to the 1993–2016 climatology for the target years [2003, 2015, 2018, 2022]. (left column, a–d) ERA5 reanalysis; (right column, e–h) SEAS5 ensemble mean.

Fig. 4.7 exhibits the observed (a-d) and predicted (e-h) soil moisture anomaly for the month of May of the four target years. The analysis of soil moisture anomalies was built on the month of May to investigate the preconditioning effect that spring soil moisture exerts on the model's summer drought forecasts. The interaction between the land surface and the atmosphere is, in fact, crucial for the development of extreme droughts.

As demonstrated by Seneviratne et al. (2010) and Fischer et al. (2007), a lack of soil moisture worsens summer droughts and heatwaves through a specific climate feedback loop: under normal conditions, a large part of the sun's energy is used to evaporate water from the soil and plants through evapotranspiration. This process turns solar energy into latent heat, which acts as a natural cooling system for the ground. However, when the soil is extremely dry, this evaporation process is severely limited; consequently, the sun's energy cannot be used for evaporation and is instead transformed into sensible heat. This type of heat directly warms the air near the surface, leading to a sharp increase in air temperatures and further drying the environment. Because of this physical process, both the final severity of a summer drought and the model's ability to predict it might depend on the initial soil moisture state.

When looking at the forecasts for May (that is, 0-month lead time), the SEAS5 model results match the observed data quite well (Fig. 4.7e-h). This high consistency is expected because the model simulations start on May 1st (as explained in Section 2.2). Additionally, the model's starting conditions come from the same ECMWF system used to create the ERA5 observations, making them naturally similar.

The ERA5 data (Fig. 4.7a-d) show that in May of all four analysed years, soil moisture was already below-normal across large parts of Europe. However, the model reacted differently depending on the year. In the May forecasts for 2003 and 2015 (Fig. 4.7e-f), the SEAS5 ensemble mean underestimated the magnitude of the negative anomaly. During the more accurately predicted droughts of 2018 and 2022, (Fig. 4.7g-h), the model forecasted intense and widespread dry soil in May. Therefore, summers that the model predicted successfully (2018 and 2022) were preceded by a forecasted initial soil moisture that was much drier compared to the summers where the model failed (2003 and 2015). By failing to capture the full

intensity of the initial soil moisture deficit, the model might have weakened the aforementioned land-atmosphere feedback loop, resulting in the underestimation of the droughts' severity.

Examining the spatial patterns more closely reveals distinct differences in the model's behaviour across the analysed years. While in 2003 the SEAS5 model primarily underestimated the overall intensity of the soil moisture deficit (Fig. 4.7a-e), its shortcomings in 2015 were also geographical (Fig. 4.7b-f). Specifically, the model failed to capture the spatial distribution of the drought, missing the extensive negative anomalies over vast areas of Central and Eastern Europe, including France, Germany, and Poland. Reanalysis data confirm that these regions were already recording lower-than-normal soil moisture values in May, acting as a possible precursor for the areas that would ultimately become the most affected ones of the severe summer drought. On the other hand, the 2018 and 2022 maps (Fig. 4.7c-g) reveal that the model correctly captured both the intensity and the location of the drought. In the 2018 summer, the extreme dry conditions impacted Central Europe and the model's May forecast correctly anticipated this pattern: normal spring soil moisture in the Mediterranean and severe negative anomalies through the central regions of the continent.

4.3.2 Air temperature at 2 metres

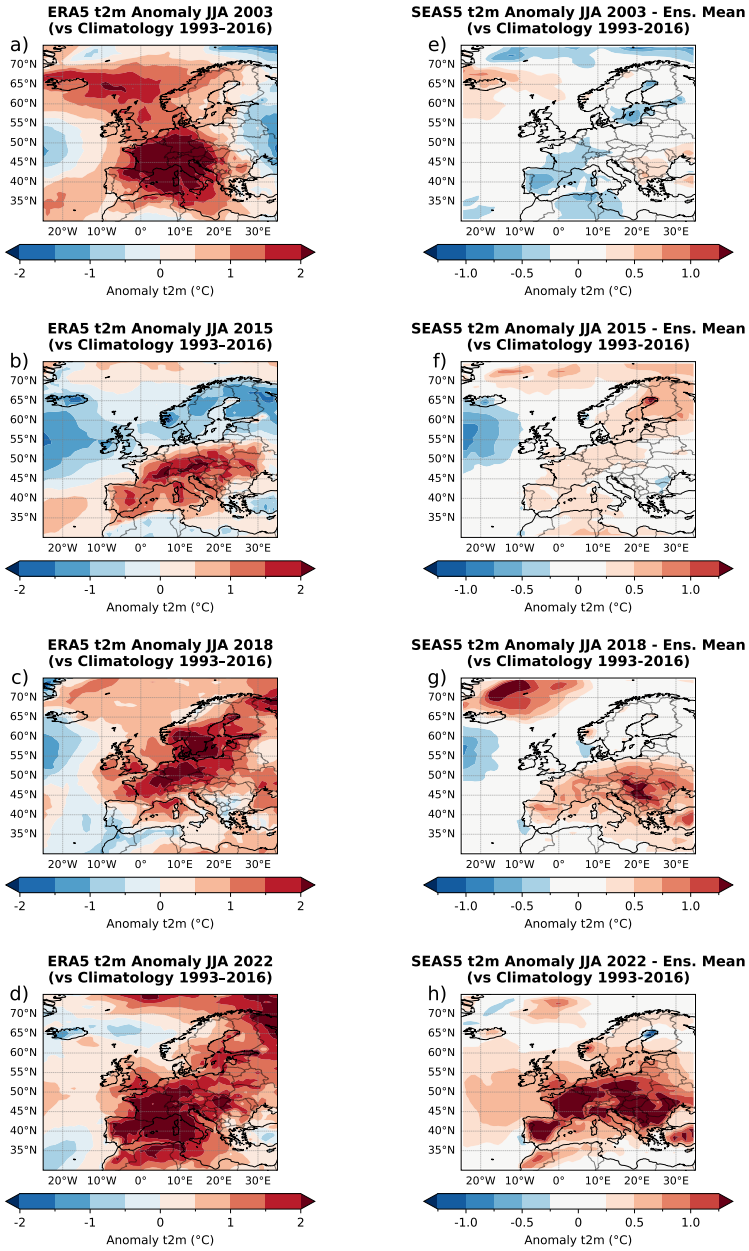

Figure 4.8: JJA 2m Air-temperature Anomalies relative to the 1993–2016 climatology for the target years [2003, 2015, 2018, 2022]. (left column, a–d) ERA5 reanalysis; (right column, e–h) SEAS5 ensemble mean.

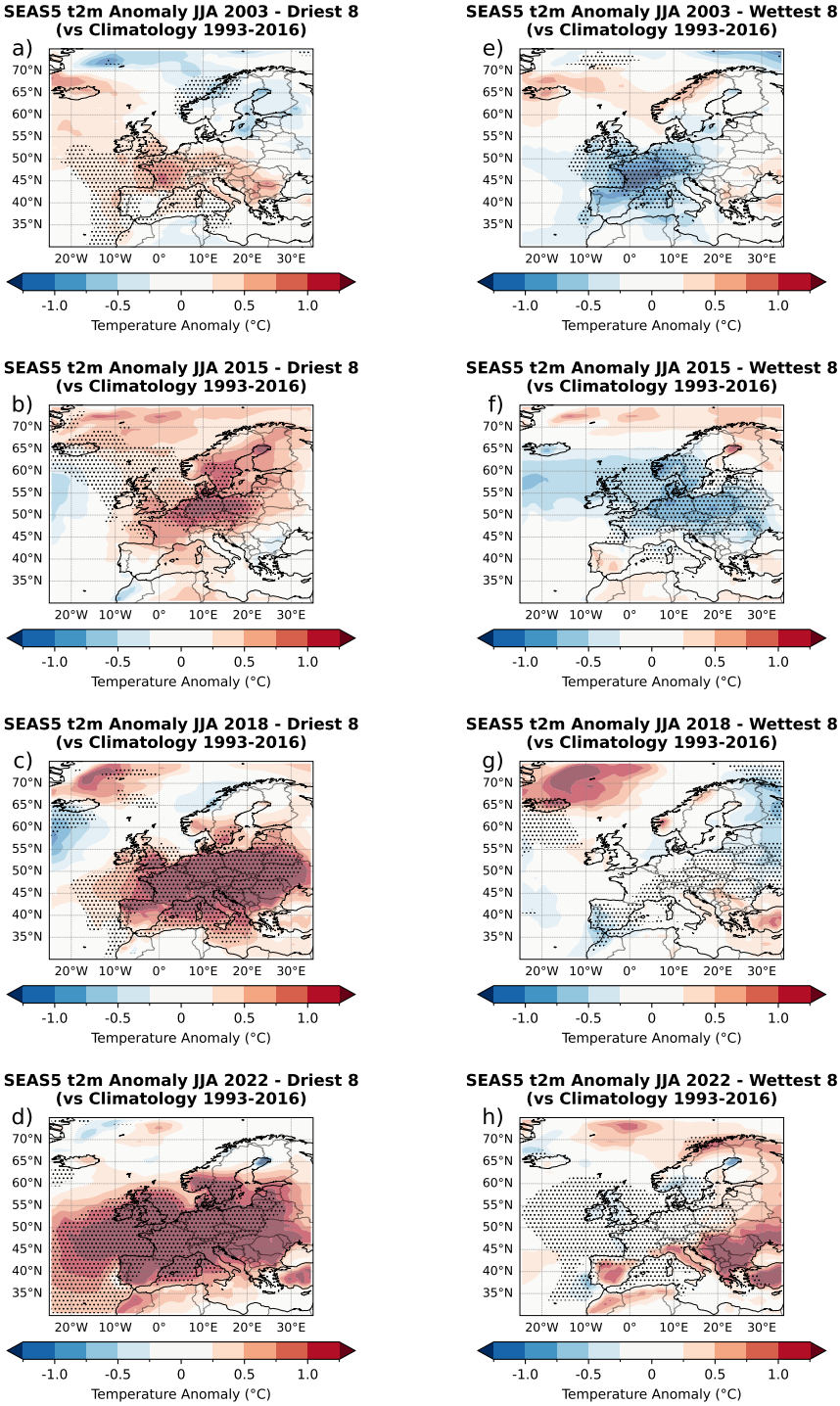

Figure 4.9: Driest (left column, a-d) and Wettest (right column, e-h) SEAS5 members t2m JJA Anomalies. Stippling indicates statistical significance at the 95% level (p value < 0.05).

Fig. 4.8 shows the observed (a-d) and predicted (e-h) t2m anomaly for the four summers under study. It should be noted that the colour bar used for the SEAS5 anomaly maps (Fig. 4.8e-h) differs from that of the ERA5 maps (Fig. 4.8a-d). This adjustment is necessary to better visualize the ensemble mean anomalies, whose extremes are inherently smoothed out. Fig. 4.9 plots the same anomaly computed for the 8 driest (a-d) and the 8 wettest (e-h) members of the model.

T2m data from ERA5 for each of the four summers (Fig. 4.8a-d) indicate pronounced positive anomalies in drought years. Fig. 4.8a shows that during summer 2003 the entire continent recorded a positive temperature anomaly, particularly the Mediterranean, France and central Europe, where the recorded temperature exceeded the expected by 2°C. Fink et al. (2004) stated that Eastern France, Northern Switzerland and alpine Germany, registered temperatures so high to exceed the JJA 1961-1990 seasonal average by 5°C. The magnitude of these temperature anomalies was exacerbated by land-atmosphere feedbacks, specifically a severe soil moisture deficit inherited from a dry winter and spring (Garcia-Herrera et al., 2010). That summer, the 1-month lead ensemble mean forecasts from SEAS5 forecasted temperatures within the normal range almost everywhere (Fig. 4.8e), except for a slight below-average temperature in Spain and France.

In the same way, ERA5 t2m data for 2015 (Fig. 4.8b) show the highest increases in the Alps and the Czech Republic, where temperatures were on average more than 2 degrees higher than usual. Conversely, higher latitudes (including the British Isles and Scandinavia) recorded slightly lower than normal temperatures that summer, deviating from the critical values registered in the southern-central part of the continent. The SEAS5 seasonal model (Fig. 4.8f), on the other hand, predicted a JJA season with temperatures in line with the average over Europe, except for eastern Scandinavia, where a slight increase was expected, which did not occur.

The difference between the poorly predicted summers of 2003 and 2015 and the well-forecasted one of 2018 is visible in Fig. 4.8c-g. ERA5 shows that during the JJA season of 2018, most of the European continent recorded higher than average temperatures, particularly Central Europe and Scandinavia. Although the intensity of the temperature increase was underestimated by the model ensemble mean, SEAS5 also predicted an above-average t2m summer across most of the continent for that season, excluding only the British Isles and Scandinavia, where

the model predicted an average summer and where, instead, high positive anomaly values over +2°C were recorded.

Summer 2022, on the other hand, represents a unique case in this study as it is the only year in which the seasonal model overestimated the severity of the drought event in its enesemble mean. Indeed, it can be observed the coherence between ERA5 (Fig. 4.8d) and forecasts (Fig. 4.8h). Both the maps exhibit strong positive anomalies across all the continent, with most of central and southern Europe with higher than +2°C values. The highest maximum temperature anomaly on record that summer was registered in Western Europe, and it was about 10°C higher than typical summer maximum temperatures (Copernicus Climate Change Service, 2023).

Overall, the analysis of Air Temperature anomalies reveals a remarkable thermodynamic difference between the driest and wettest members of the SEAS5 ensemble. As shown in Fig. 4.9a-d, for all the four summers the driest members—defined by their ability to predict low water balance values—consistently exhibit statistically significant positive t2m anomalies coinciding with the drought-affected regions. On the other hand, the wettest members are characterized by significant neutral or negative temperature anomalies (Fig. 4.9e-h). This pattern indicates that the predictability of the drought signal in SEAS5 is linked to the model's ability to capture the associated heat extreme. Physically, this relationship might suggest a key role for evapotranspiration in driving the summer water deficit. The higher temperatures predicted by the driest members increase the vapor pressure deficit, thereby enhancing atmospheric evaporative demand, possibly accelerating soil moisture depletion (Seneviratne et al., 2010).

The maps of the wettest members in 2003 and 2015 (Fig. 4.9e-f) show much more pronounced negative anomalies than the worst ones in 2018 and 2022 (Fig. 4.9g-h), which had predicted an average summer rather than cooler. A remarkable feature of the driest members in poorly predicted summers (Fig. 4.9a-b) is that even near-average values (the white areas in Fig. 4.9a-b) are statistically significant. The same occurs for the wettest members in well-predicted summers (Fig. 4.9g-h). This implies that when the model missed the extreme heat, predicting a normal summer was already an extreme behaviour within the ensemble. On the other hand, when the model correctly predicted an extreme summer, the members forecasting

normal conditions deviated the most from the ensemble mean, thus becoming statistically significant.

4.3.3 Total Precipitation

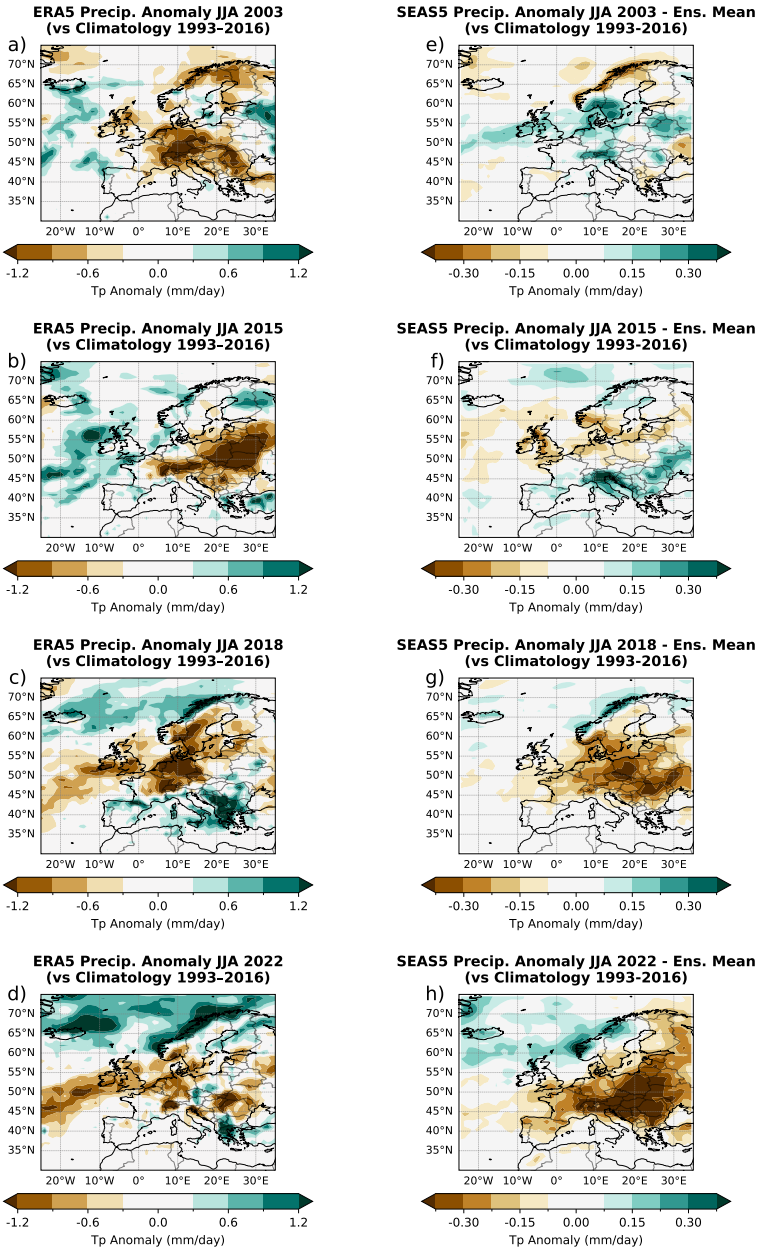

Figure 4.10: JJA Total Precipitation Anomalies relative to the 1993–2016 climatology for the target years [2003, 2015, 2018, 2022]. (left column, a–d) ERA5 reanalysis; (right column, e–h) SEAS5 ensemble mean.

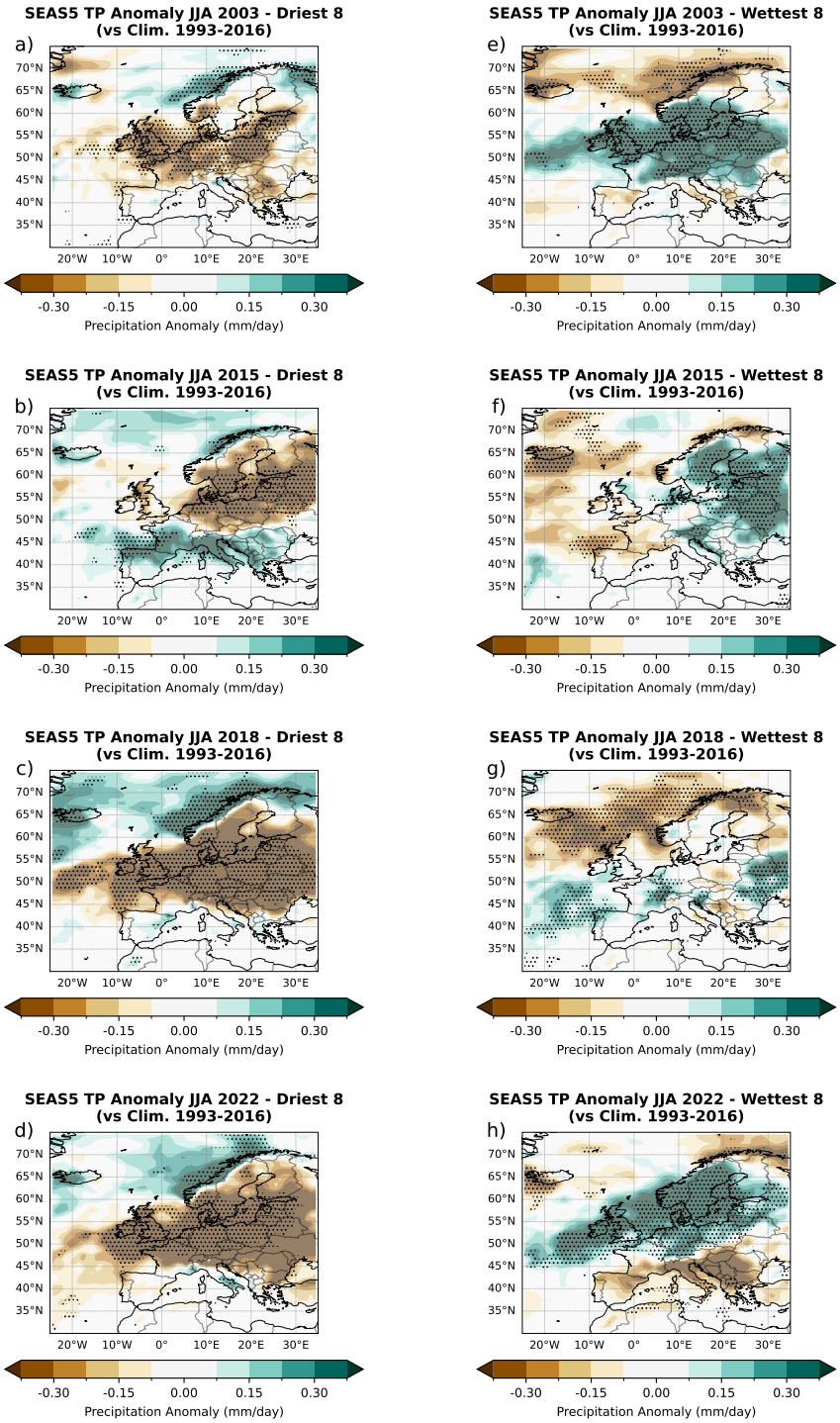

Figure 4.11: Driest (left column, a-d) and Wettest (right column, e-h) SEAS5 members Tp JJA Anomalies. Stippling indicates statistical significance at the 95% level (p value < 0.05).

Analogously to t2m, Fig. 4.10 shows the observed (a-d) and predicted (e-h) tp anomaly for the four summers here analysed. For the same reason explained in Section 4.3.2, the colour bar used for the SEAS5 anomaly maps (Fig. 4.10e-h) differs from that of the ERA5 maps (Fig. 4.10a-d). Fig. 4.11 exhibits the same anomaly averaged for the 8 driest (a-d) and the 8 wettest (e-h) members of the ensemble.

The analysis of observed precipitation anomalies (Fig. 4.10a-d) confirms a general, severe deficit in rainfall compared to the reference climatology, acting as a contributing driver for the corresponding drought occurrence. During summer 2003, the most severe deficits (exceeding -1.2 mm/day) were recorded in France, Switzerland, and the Alpine region of Germany (Fig. 4.10a). This localized lack of precipitation mirrors the highest t2m anomalies (Fig. 4.8a). However, the SEAS5 ensemble mean failed to capture this localized anomaly (Fig. 4.10e), predicting above-normal rainfall for the Alps—one of the regions hardest hit by the drought.

The ERA5 and SEAS5 maps for 2015 (Fig. 4.10b-f) show large discrepancies. While ERA5 reported central-eastern Europe as the area most affected by drought during that summer – and the UK and Scandinavia as the least affected – the model predicted positive anomalies in central-eastern Europe and negative anomalies in the British Isles and Scandinavia, in line with the predicted pressure pattern which foresaw a High over these regions. The 2015 event was characterized by a sharp meridional contrast between a severely dry central-eastern Europe and an anomalously wet Mediterranean (Fig. 4.10b). The driest members successfully captured this dichotomy (Fig. 4.11b), accurately predicting the wet anomaly in the Mediterranean basin. However, the overall forecast accuracy remains limited, since only a small fraction of ensemble members reproduced the event correctly, indicating a large ensemble spread.

As for 2018, the model's ensemble mean shows widespread dry anomalies in central and northern Europe, despite failing to predict a wetter-than-normal conditions in the eastern Mediterranean (Fig. 4.10g).

A different forecasting bias emerged during the summer of 2022. While SEAS5 successfully anticipated the continental drought, it tended to overestimate its negative impact and spatial spread, expecting a severe lack of precipitation over all of Europe, with the most intense deficits projected for the central-eastern regions

(Fig. 4.10h). ERA5 (Fig. 4.10d), revealed that severe precipitation deficits were concentrated over the Alps, Germany, and the British Isles. Notably, despite the general overestimation of the event across the continent, the British Isles remained the only region where SEAS5 underestimated the severity of the drought - consistent with the high BS values previously calculated for that area.

In align with the t2m diagnostics, Fig. 4.11 shows that the driest members are characterized by statistically significant negative precipitation anomalies that align with the observed drought cores and significant positive anomalies that align with those areas less affected by the drought. Conversely, the wettest members exhibit significant neutral or positive anomalies in the regions effectively affected by the drought and significant negative anomalies in the least affected areas, highlighting their failure to capture the observed summer precipitation patterns.

4.3.4 Mean Sea Level Pressure

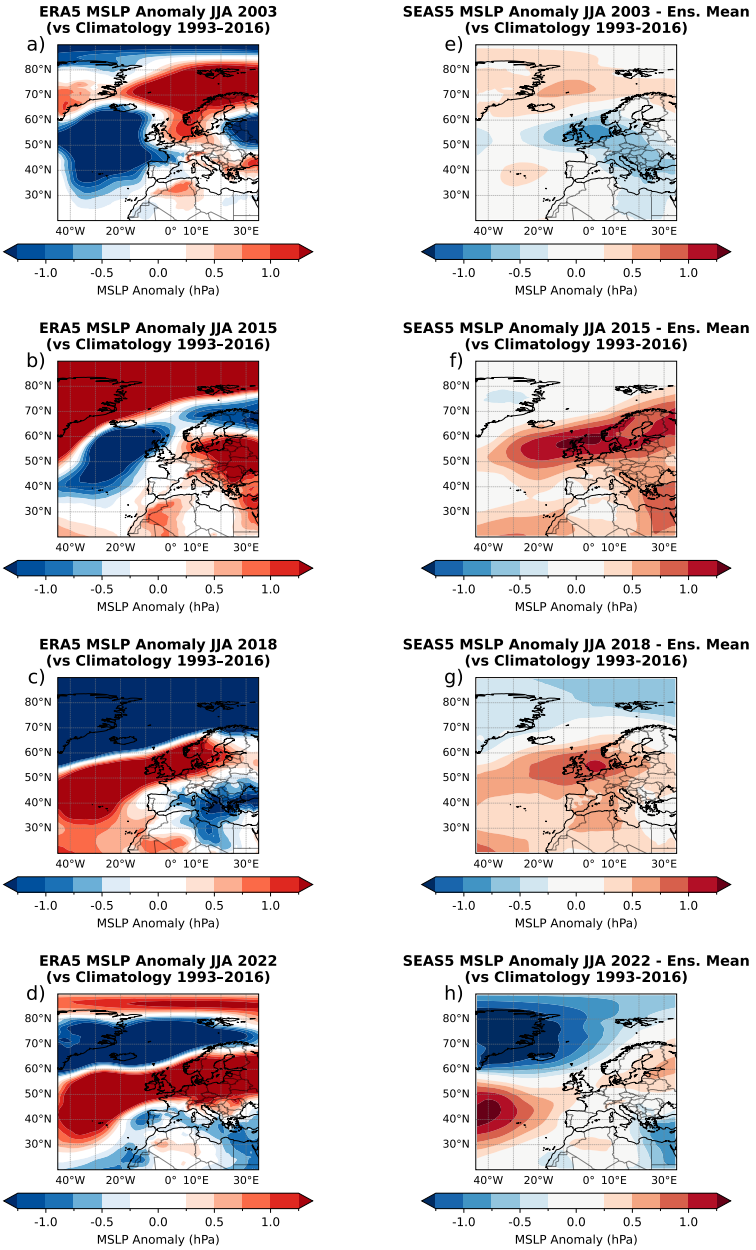

Figure 4.12: JJA Mean Sea Level Pressure Anomalies relative to the 1993–2016 climatology for the target years [2003, 2015, 2018, 2022]. (left column, a–d) ERA5 reanalysis; (right column, e–h) SEAS5 ensemble mean.

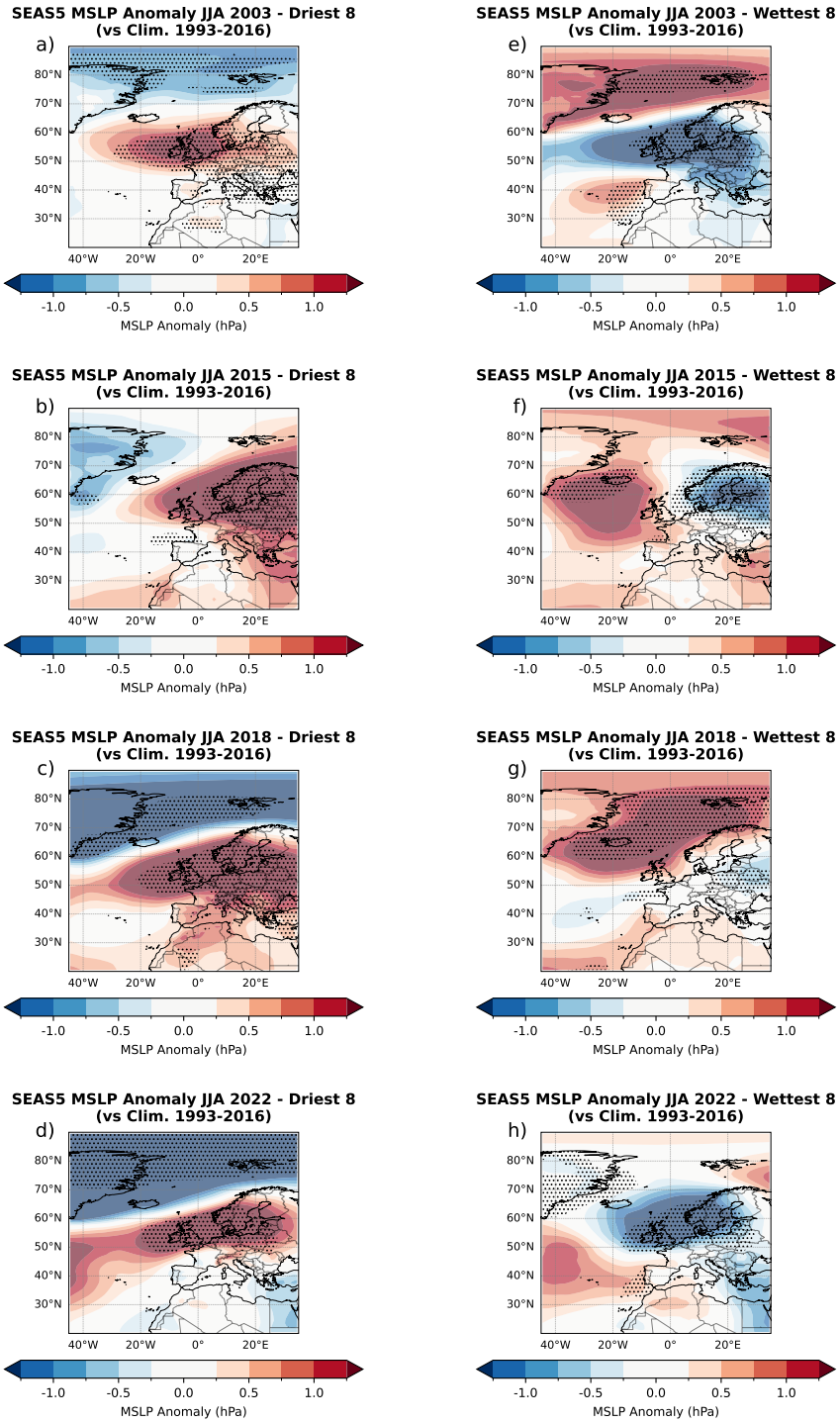

Figure 4.13: Driest (left column, a-d) and Wettest (right column, e-h) SEAS5 members MSLP JJA Anomalies. Stippling indicates statistical significance at the 95% level (p value < 0.05).

The MSLP summer anomalies are shown in Fig. 4.12, both the observed (a-d) and predicted (e-h) by the ensemble mean. Later, the average anomalies of the 8 driest (a-d) and the 8 wettest (e-h) members were computed and plotted in Fig. 4.13.

The comparison between ERA5 reanalysis and SEAS5 seasonal forecasts for MSLP reveals distinct synoptic drivers across the four summers, characterized by opposing phases of the Summer North Atlantic Oscillation (SNAO). For instance, MSLP data from ERA5 indicate that the summers of 2003 and 2015 were characterized by a negative SNAO phase (Fig. 4.12a-b), featuring higher pressure over Arctic/Greenland and lower pressure relative to the British Isles and the North Atlantic. Conversely, the summers of 2018 and 2022 exhibited a robust positive SNAO configuration, defined by deep low pressure over Greenland and high pressure centred over the British Isles and Scandinavia (Fig. 4.12c-d).

Despite the shared negative SNAO background, the 2003 and 2015 events manifested through distinct blocking mechanisms that the model struggled to reproduce. In 2003, the observed MSLP anomaly exhibited a robust dipole-like structure reminiscent of a blocking regime: a pronounced negative anomaly over the North Atlantic contrasted with a stationary blocking anticyclone extending from Scandinavia to Central Europe (Fig. 4.12a). This configuration reflects the presence of a stationary high pressure system that persisted throughout much of the season (Black et al., 2004). This pressure setup resulted in a large-scale subsidence, inhibiting cloud formation and maximizing surface solar irradiance (Fink et al., 2004). According to Garcia-Herrera et al. (2010), the 2003 atmospheric blocking was caused by an anomalously persistent northerly displacement of the Atlantic Subtropical High, rather than a standard blocking pattern. Furthermore, the pressure gradient between the Atlantic trough and the continental high generated a persistent southerly flow bearer of hot air from North Africa and the Iberian Peninsula into France and Central Europe (Garcia-Herrera et al., 2010). Notably, a positive anomaly of approximately 1 hPa was registered over the Alps during the same summer, which coincided with a 5-10% reduction in the total mass of the region's ice cover. The seasonal model ensemble mean failed to foresee this anomalous pressure configuration, by predicting a low-pressure area right where the droughts had the most impacts.

Similarly to 2003, the 2015 event was driven by a distinct zonal pressure dipole. ERA5 data (Fig. 4.12b) displays a deep negative anomaly south of Iceland paired with a blocking ridge over Central-Eastern Europe. As hypothesized by Duchez et al. (2016), the anomalously cold North Atlantic SST registered during summer 2015 could have forced a stationary meander of the Jet Stream. This manifested as a deep trough over the Atlantic paired with a blocking ridge over Europe, which facilitated an intense meridional advection of subtropical air. Once established, the high-pressure system triggered a positive feedback loop: clear skies increased surface heating, which in turn reinforced the high-pressure centre (Ionita et al., 2017), creating a dynamical barrier that diverted Atlantic lows towards Scandinavia.

In contrast to the earlier events, Fig. 4.12c-d highlight that the summers of 2018 and 2022 were driven by a positive SNAO phase, and the SEAS5 model demonstrated significantly higher predictive skill for these years. Both ERA5 and SEAS5 identified for the JJA season of 2018 a robust positive MSLP anomaly centred over the British Isles and Scandinavia (Fig. 4.12c-g). The 2018 synoptic framework was characterized by a North-South dipole of a Scandinavian blocking ridge at northern latitudes and a low-pressure zone over the Eastern Mediterranean and the Balkans. This configuration aligns with the observed precipitation anomalies, which registered a drier JJA season in correspondence to the Scandinavian High, and a wetter-than-normal summer for the Mediterranean region, especially the Balkans. This type of atmospheric circulation was characterized by the typical configuration of a positive SNAO phase with the setup of a double jet stream (Rousi et al., 2023). The establishment of the double jet stream is increasingly attributed to Arctic Amplification (Coumou et al., 2018). As the Arctic region warms at a faster rate than the mid-latitudes, the Equator-to-Pole temperature difference (a key driver of zonal winds) is reduced. This weakening of the thermal gradient causes the main polar jet to lose momentum, becoming wavier and more prone to bifurcation. The resulting double jet architecture is a critical driver of blocking events: the separation of the zonal flow into two distinct branches (one at high latitudes and one at low latitudes) creates a dynamic environment where high-pressure systems become trapped between the jets. In the case of summer 2018, the Scandinavian High remained “trapped” between the Mediterranean and the polar low-pressure zones. This mechanism effectively “locks” the synoptic

pattern, stalling the weather for weeks and allowing extreme heat to accumulate over the continent (Rousi et al., 2023).

The atmospheric pattern of the observed MSLP during summer 2022 is very similar to that of 2018. The ERA5 map (Fig. 4.12d) show indeed a North-South dipole with a Scandinavian blocking ridge covering most of the Northern latitudes and a Southern low-pressure zone above the Iberian Peninsula and Greece. Unlike 2018, while the model ensemble mean correctly identified the North-South dipole structure, it underestimated its intensity (Fig. 4.12h).

The comparative analysis of MSLP anomalies of the four summers under examination reveals that the SEAS5 model's ability to predict the European drought is likely dependent on its capacity to capture the correct SNAO phase and the specific geometry of high-latitude blocking. This outcome arises from the observed common pattern that links the behaviour of the driest and wettest members for each of the four summers. Members that successfully predicted the drought (Fig. 4.13a-d), usually display a significant pressure dipole with a Low over the Arctic/Greenland and a High over UK/Central-Northern Europe, corresponding to the positive phase of the SNAO (Folland et al. 2009). The deep low-pressure anomaly over the Polar region could strengthen the meridional pressure gradient, allowing the Subtropical High to expand northward and a stable blocking-like regime to establish over the continent, shielding Europe from Atlantic inflow (Bladé et al., 2012). Consistently, a positive SNAO phase is associated with a northward shift of the North Atlantic storm track, resulting in dry conditions over Central-Northern Europe (Folland et al., 2009). Furthermore, the enhanced meridional gradient between the Arctic and the Subtropics observed in the driest members may accelerate the zonal westerly flow and suppresses meandering, effectively confining the storm track to high latitudes and preventing the intrusion of moist air into the continent (Coumou et al.2018). The combination of these two factors can make the model foresee the drought event.

Conversely, the wettest members exhibit typical negative or close-to-neutral SNAO configurations (Fig. 4.13e-h), generally predicting high-pressure over Greenland and the Arctic, and low-pressure over the Northern regions of the continent. According to Hurrell et al. (2003), the presence of high pressure at the pole could lead to the southward displacement of the storm track. This configuration, typical

of the negative SNAO phase, could have led the model to foresee depressions directly into Central Europe, resulting in the significant wet bias observed in the failed forecasts of Summer 2003 and 2015.

To check if the seasonal forecasts of SEAS5 are influenced by the expected SNAO phase, the SNAO index was calculated for each case according to the method proposed by Folland et al. (2009). The index represents the difference in normalized MSLP between the southern node located over United Kingdom and the northern node located over Greenland. In Tab. 4.1, the SNAO indices for the four target dry summers are shown.

Anno	**ERA5 (May)**	**ERA5 (JJA)**	**SEAS5 Ensemble Mean (JJA)**	**Driest 8 (JJA)**	**Wettest 8 (JJA)**
2003	0.89	-0.46	-0.59	1.02	-1.90
2015	1.77	-1.04	0.54	0.94	-0.03
2018	4.59	2.86	0.74	2.48	-0.43
2022	2.44	2.36	0.91	2.19	-0.61

Table 4.1: SNAO Index computed for the target summers with ERA5 (both May and JJA), SEAS5 ensemble mean and SEAS5 driest and wettest members.

According to Tab. 4.1, the poorly predicted summers of 2003 and 2015 have recorded negative SNAO phase (-0.46 and -1.04 respectively), while the more accurately-predicted summers of 2018 and 2022 were characterized by a positive phase (2.86 and 2.36 respectively). This result suggests that a correlation between the SNAO and the European summer drought predictability might exist, and the model tends to more accurately predict droughts arising from a positive SNAO phase. Conversely, the model struggles to predict a high-pressure block in summer that is not centred on the United Kingdom (as happened in 2003 and 2015) and droughts are not well-represented by SEAS5 under negative SNAO phases.

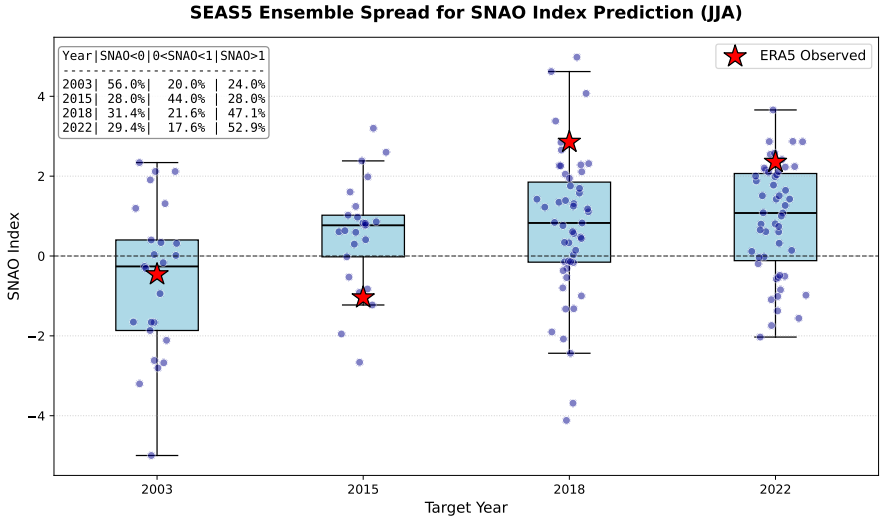

Figure 4.14: SEAS5 ensemble spread for the SNAO index forecast for the four target years. Red stars indicate the recorded SNAO index according to ERA5 reanalysis. Text box exhibits the percentage of members predicting SNAO < 0, $0 <$ SNAO < 1, and SNAO> 1 for the target summers.

Fig. 4.14 shows the spread of the model's ensemble for the SNAO index prediction in the different target summers. For 2018 and 2022, the ensemble mean successfully reproduces the positive sign of the anomaly (+0.74 and +0.91, respectively), indicating strong agreement among ensemble members (Fig. 4.14). However, despite correct directional guidance, the ensemble mean underestimate the amplitude of the real event, which doubled the simulated intensity. While the members strongly agree on forecasting a positive SNAO (68.6% for 2018 and 70.6% for 2022), the members which predicted a strong positive SNAO are fewer (only

47.1% for 2018 and 52.9% for 2022).

The text box in Fig. 4.14 highlights the greater uncertainty for the 2003 SNAO forecasts, as the members are almost equally divided between positive and negative forecasts (56% of the ensemble predicted a negative SNAO < 0 and 44% a positive SNAO), indicating a high dispersion and low coherence within the ensemble. In 2015 the ensemble mean predicts a slightly positive index (+0.54) with great consistency of the ensemble (72% of the total members, but only 28% of them greater than 1), whereas the observed value was strongly negative (-1.04). As shown in the SWBA analysis (Fig. 4.3b-f), the ensemble mean predicted a typical positive SNAO phase with dry conditions in northern Europe and wet condition in central and southern regions. However, in 2015, the drought occurred mostly in the central-eastern Europe with a blocking high simultaneous with a negative SNAO phase.

The 2003 case is illustrative of internal model uncertainty: despite being a poorly predicted summer, the model ensemble mean correctly captured the negative SNAO phase (-0.59 predicted and -0.46 observed). This suggests that the model struggles to represent blocking systems during negative SNAO phases. The examination of the SEAS5 driest members reveals the reliance on the positive SNAO phase to generate drought within the model outputs. Regardless of the observed state, the driest members consistently simulated positive SNAO pshase across all four years (Tab. 4.1). In 2018 and 2022, the driest members simulated indices of +2.48 and +2.19 (mean on the 8 members), effectively reproducing a blocking-like pattern. Here, the model's tendency to link dry conditions with a positive SNAO phase coincided with the observed atmospheric state, improving its performance.

However, in 2003 and 2015, the same mechanism led those members to simulate droughts, but for the wrong reason. Despite the observed negative circulation anomalies, these members generated drought conditions by simulating a positive SNAO structure (+1.02 in 2003 and +0.94 in 2015). This demonstrates that the model struggles to reproduce summer droughts arising during a negative SNAO phase. The only members simulating drier-than-usual conditions also produce a positive SNAO phase and therefore fail to reproduce the actual blocking pattern.

In the end, the SNAO indices computed for the wettest members highlight the model's coupling between the negative phase with the rise in precipitation

trough the central and northern part of the continent. In 2018 and 2022, the wettest members predicted negative indices (-0.43 and -0.61 respectively), thereby missing the anomalous pressure configuration that is critical for reproducing dry summers. A different failure mode emerges in 2015, where 72% of the ensemble members agreed on a positive SNAO (Fig. 4.14). While ERA5 recorded a robust negative index (-1.04), the wettest members projected an almost neutral SNAO (-0.03), highlighting the ensemble's limitation in reproducing the strong negative phase required to match the observed conditions. The 2003 case offers the most critical insight into the model's limitations. For that summer, the wettest members predicted the negative SNAO signal (-1.90). Therefore, despite forecasting the correct SNAO phase itself, the model was unable to resolve the local blocking regime that drive the dry conditions, confirming the SEAS5 limitation in simulating summer droughts that are not associated with a positive SNAO phase.

Finally, we investigated whether the SNAO preceding the summer season constitutes a potential source of predictability. Tab. 4.1 reports the observed May SNAO index values for the target years. Notably, all the values are positive. This implies that even the summers characterized by a negative SNAO were preceded by a positive phase in spring. The main difference is the signal magnitude: 2018 and 2022 show stronger positive signals (4.59 and 2.44, respectively) compared to 2003 and 2015 (0.89 and 1.77). This suggests that the positive May SNAO, common to all these dry summers, may have contributed to preconditioning the soil during spring, exacerbating the initial water deficit and depleting soil moisture. Interestingly, the more accurately predicted years were associated with a more extreme SNAO phase, likely generating the broader soil moisture anomalies shown in Fig. 4.7. Following Dunstone et al. 2019, who suggested that for the summer of 2018 soil moisture anomalies alone could not explain the intensity of the forecasted drying signal, the next section aims to investigate whether specific SST patterns, when present, may have influeced the forecasts by preconditioning the atmosphere towards drought-prone conditions.

4.3.5 Sea Surface Temperature

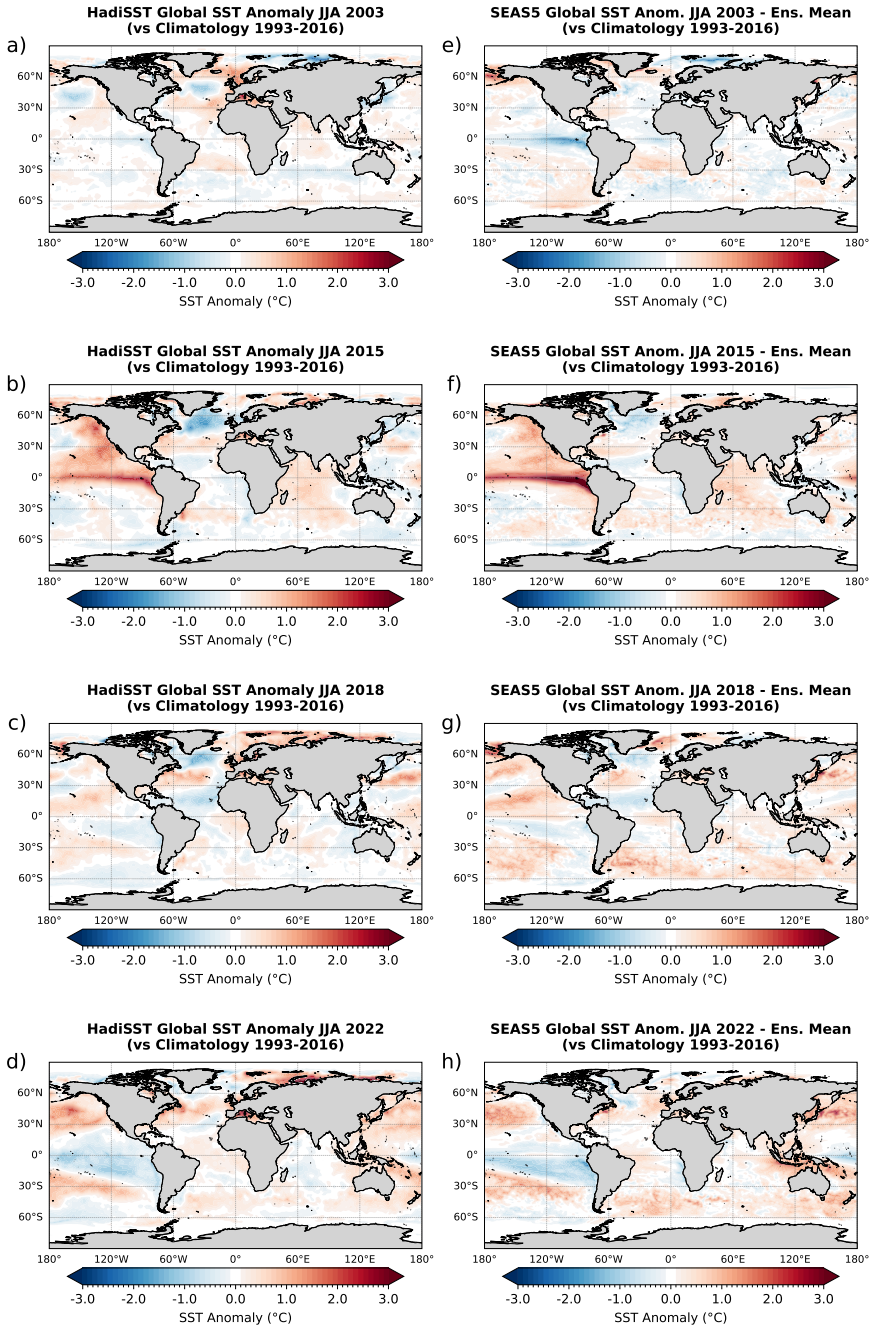

Figure 4.15: JJA Sea Surface Temperature Anomalies relative to the 1993–2016 climatology for the target years [2003, 2015, 2018, 2022]. (left column, a–d) HadiSST observations; (right column, e–h) SEAS5 ensemble mean.

Fig. 4.15 shows observed (a-d) and predicted (e-h) JJA SST anomalies for the target years [2003, 2015, 2018, 2022]. Fig. 4.15a-e shows SST anomalies for the summer of 2003, highlighting that the model predicted a strong La Niña signal (strongly negative SST anomalies in the Eastern Pacific). Although Patterson et al. (2022) suggest that La Niña conditions typically favour a northward shift of the jet stream and anticyclonic anomalies over the Euro-Atlantic sector, the SEAS5 hindcast failed to reproduce the observed blocking pattern in its ensemble mean. However, a member-by-member analysis would be more appropriate to assess whether and where blocking emerged in individual ensemble members, and whether such blocking is linked to the negative ENSO phase. As previously established, the 2003 heatwave was sustained by a northward displacement of the Atlantic Subtropical High and further amplified by a severe soil moisture deficit originating in spring (Fig. 4.7). In the ensemble mean, the blocking signal might disappear due to averaging of different circulation anomalies across individual members, while the model itself may also underestimated the local thermodynamic land-atmosphere feedback, thereby failing to systematically establish the stationary high-pressure ridge despite the large-scale ENSO signal.

A possible limitation of SEAS5 model in 2015 (Fig. 4.15b-f) was the poor representation of extremely cold SSTs across the North Atlantic. Duchez et al. (2016) shows that these cold temperatures are the most extreme cold conditions in the modern record for the mid-high latitude North-East Atlantic (a pattern commonly observed prior to severe European heatwaves since 1980). Observations for summer 2015 (Fig. 4.15b) exhibit a strong cold anomaly in the subpolar North Atlantic (SPNA), other than a strong positive ENSO signal (El Niño) in the Pacific. ENSO is known to be the driver of many climatologic patterns across the globe (McPhaden et al., 2006) but the correlation between El Niño phase and summer heatwaves in Europe it is still debated (Mecking et al., 2019). However, the study conducted by Mecking et al. (2019) on the influence of this positive ENSO signal on the drought of 2015 stated that the heatwave was influenced by the combination and coexistence of local patterns (the “cold blob” in the North Atlantic) and remote patterns (positive ENSO signal). By omitting one or the other in the model initialization, the output would have been only half of the intensity of the heatwave. Despite overestimating the positive ENSO signal, the SEAS5 model ensemble (Fig.

4.15f) underestimated the extreme "cold blob" recorded prior and during summer 2015, resulting in a more tempered forecast of a typical European summer.

Summer 2018 observation map (Fig. 4.15c) show a strong SST gradient between the subpolare gyre and the Gulf Stream path, other than warm anomalies in the Mediterranean. The ensemble mean appears to have successfully captured these oceanic conditions (Fig. 4.15g).

The oceanic configuration of summer 2022 was characterized by a relevant marine heatwave in the Mediterranean basin and a strong negative ENSO signal (Fig. 4.15d). Indeed, the Mediterranean Sea experienced a record-breaking marine heatwave, and average European SSTs were the warmest on record (Copernicus Climate Change Service, 2023). Unlike previous years, no cold blob was observed or predicted; instead, SSTs around the UK and western Europe were warmer than average, potentially warming western Europe via thermal advection (Patterson et al., 2024). Furthermore, 2022 was the third consecutive year of La Niña (as the negative SST anomalies over the Eastern Pacific suggest in Fig. 4.15d-h), which is usually associated with anticyclonic conditions over the North Atlantic (coherent with HadiSST observations) and with a northward shift of the jet stream (Patterson et al., 2024). The latter can be a driver of summer drought in Europe: acting as the main waveguide for synoptic-scale disturbances, its poleward displacement redirects the Atlantic storm track towards higher latitudes (e.g., Iceland and Northern Scandinavia), depriving Central and Southern Europe of precipitation (Patterson et al., 2024). This dynamic void facilitates the northward expansion of subtropical high-pressure systems (specifically the Azores High in 2022) and the establishment of blocking anticyclones over the continent (Copernicus Climate Change Service, 2023). The seasonal model well-predicted this northward shift of the jet stream but, according to the research conducted by Patterson et al. in 2024, it is crucial to distinguish between the physical driver of the 2022 event and the predictive skill of the SEAS5 model. Physically, the phenomenon can be associated with the persistent La Niña conditions, but the SEAS5 model exhibits a systematic bias: it simulates a long-term northward trend of the summer jet in response to anthropogenic forcing, which contradicts historical observations that show a slight southward migration over recent decades (Patterson et al., 2024). Therefore, the accurate prediction of the 2022 jet shift was likely a combination between

the real forcing from La Niña and the model's inherent tendency to shift the jet poleward under warming scenarios. However, the model predicted for that summer an even reinforced negative SST anomaly across the eastern Pacific (Fig. 4.15h), meaning that the prediction of the northward shift of the jet stream could have been driven also by the expectations of a stronger negative ENSO phase, which could be considered as a source of predictability.

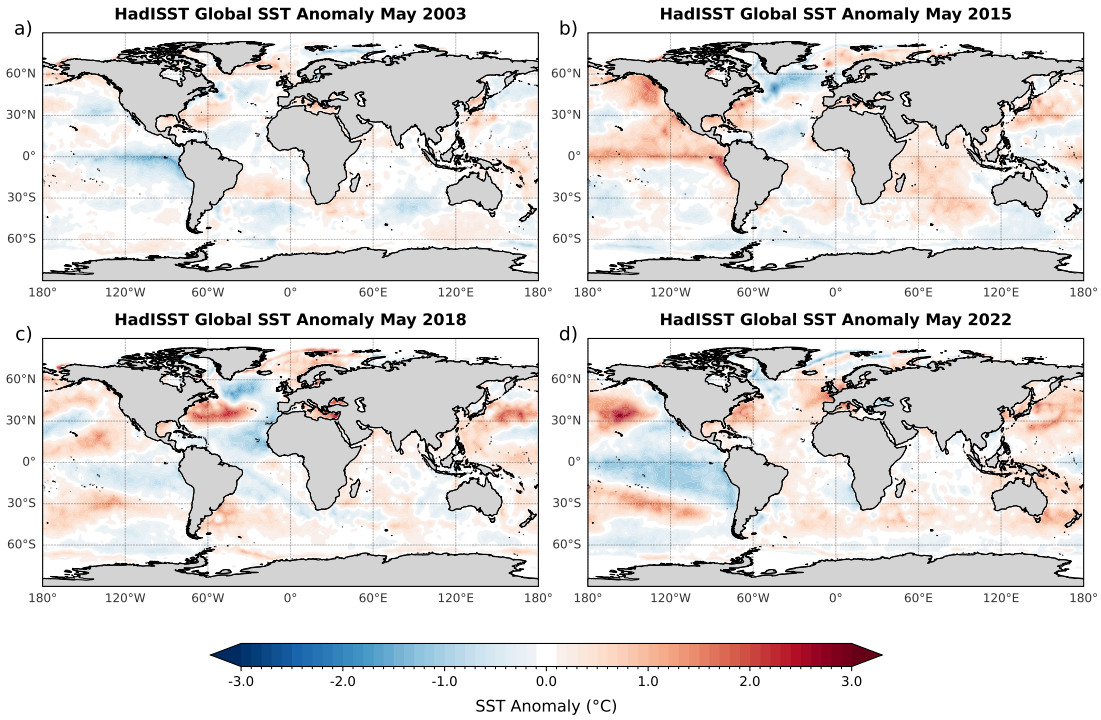

Figure 4.16: Observed (HadiSST) May SST anomalies relative to the 1993–2016 climatology for the target years [2003, 2015, 2018, 2022].

Fig. 4.16 shows observed May SST anomalies for the target years [2003, 2015, 2018, 2022]. As previously said, cold SST in the SPNA strengthen the meridional SST gradient, acting as a precursor for summer droughts by forcing the Jet Stream to meander northward and lock into a stationary anticyclonic pattern (Duchez et al. 2016, Ossò et al. 2018), thereby being a possible source of droughts predictability. Notably, the aforementioned strong SST gradient has been recorded prior to the well-predicted summer of 2018 according to HadiSST (Fig. 4.16c). On contrary, a

visual inspection suggests that the meridional SST gradient (e.g. between the cold anomalies in the SPNA and the Gulf Stream) is weaker in the ensemble mean for both 2003 and 2015, possibly contributing to the model's difficulty in representing a meandered and stationary jet.

The other common feature observed in the May anomaly maps for 2018 and 2022 (Fig. 4.16c-d) is the strong warming of the Mediterranean, suggesting it as a potential source of droughts predictability.

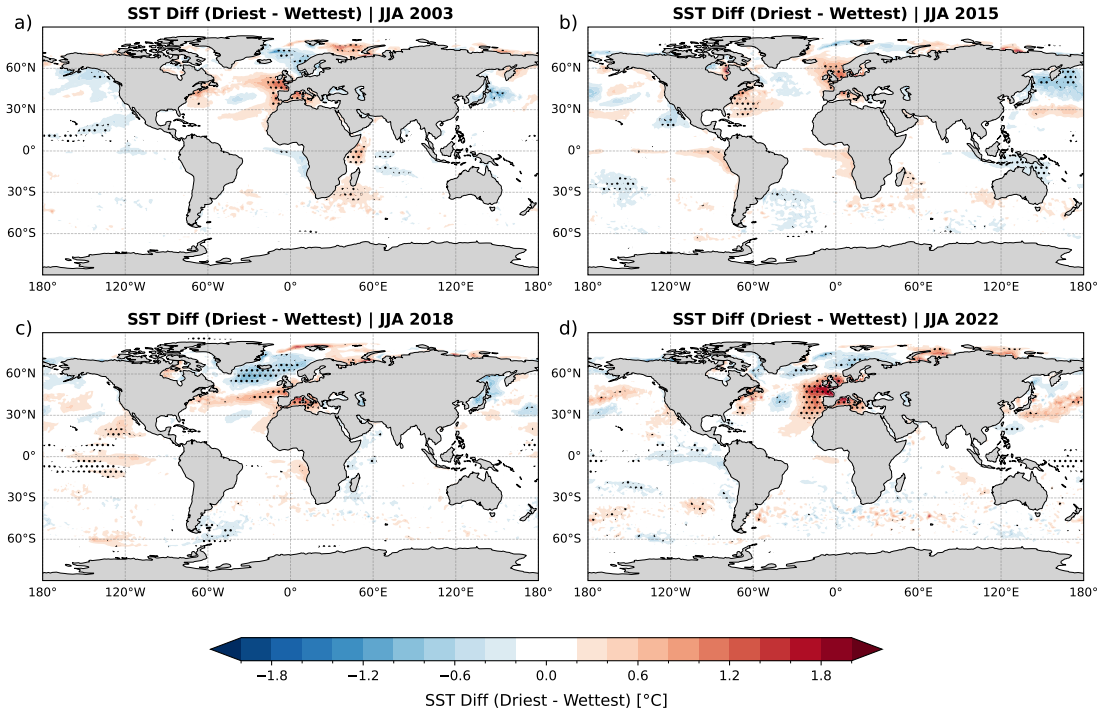

Figure 4.17: SST Driest - Wettest SEAS5 members. Stippling indicates statistical significance at the 95% level (p-value < 0.05).

For SST, statistical significance was calculated based on the difference between the eight driest- and eight wettest members. This approach was chosen to highlight with greater clarity the specific oceanic patterns associated with successful drought prediction. The resulting patterns suggest that the model's predictive skill for European summer droughts is closely tied to distinct oceanic drivers, which vary depending on the dynamical nature of each heatwave event.

Figure 4.17 shows the SSTs difference between the driest and the wettest SEAS5

members, where stippling indicates statistical significance at the 95% level. Across all analysed summer seasons, the driest members consistently exhibit significantly warmer SSTs in the Mediterranean basin and the Northeast Atlantic—immediately off the coasts of Europe—compared to the wettest members, possibly being a critical prerequisite for drought forecasting skill in all cases. Indeed, anomalously warm seas can initiate a thermodynamic positive feedback loop essential for sustaining a heatwave (Feudale and Shukla, 2011). The warmed ocean acts as a thermal reservoir, continuously releasing heat into the overlying atmosphere. This upward energy flux thermally expands the air column, effectively stabilizing the anticyclonic circulation and anchoring the high-pressure system over the region (Feudale and Shukla, 2011). This warm anomaly was observed in May during all four summers, albeit with greater intensity in 2018 and 2022 (Fig. 4.16c-d). This feature, coupled with the agreement among the driest members regarding its significance, positions this anomaly as a potential source of drought predictability.

Another common significant signal is the presence of colder SSTs in the SPNA, specifically in the region extending from Greenland to Scandinavia, as observed in the maps for 2003, 2018, and 2022 (Fig. 4.17a-c-d). This significant cold signal-and the related SST gradient-is particularly pronounced in 2018, underscoring the potentiality of the "cold blob" as a source of summer drought predictability. Consequently, a statistically significant dipole pattern emerges in these three years: the driest members consistently predict warmer conditions in the Mediterranean coupled with significantly colder SSTs in the subpolar North Atlantic. Ossó et al. (2018) demonstrated that cold SST anomalies in this region enhance the meridional temperature gradient, favouring a positive SNAO phase and a northward displacement of the jet stream, ultimately resulting in the forecast of dry conditions over Central-Northern Europe. In other words, by simulating these colder temperatures, the driest members likely facilitated the necessary northward shift of the storm track, thereby allowing stable anticyclonic conditions to establish over Central Europe. While cold blobs were actually recorded in summers 2003 and 2018 (Fig. 4.15a-c), observational data for 2022 show no particular cold anomalies in the SPNA (Fig. 4.15d). It is likely that the members who predicted the drought expected it to occur in conjunction with a "cold blob" phenomenon, which did not actually happen and that is not even relevant in the 2022 model's ensemble mean (Fig.

4.15h).

Distinctly, the 2015 significance analysis diverges from the patterns observed in the other three years, as the driest members lack of a significant cold SST anomaly in the SPNA (Fig. 4.17b). This divergence suggests that the predictive skill for the 2015 summer drought did not rely on the high-latitude blocking dynamics typically associated with the subpolar trough. Instead, the successful ensemble members were distinguished by a significant warm anomaly in the Western Atlantic, extending from the Caribbean to the US East Coast along the path of the Gulf Stream. The presence of this warm signal suggests that the atmospheric circulation over Europe was likely influenced by mid-latitude oceanic forcing rather than the positive ENSO teleconnection, which does not register any significance in this test. Minobe et al. (2008) argued that the sharp SST gradients and warm waters along the US East Coast drive surface convergence and upward vertical motion that can penetrate deep into the free troposphere. This deep diabatic heating can effectively anchor atmospheric planetary waves, known as Rossby waves. Furthermore, Sutton and Dong (2012) emphasize that summer climate anomalies in Europe are often linked to the downstream propagation of these stationary Rossby waves originating from the Western North Atlantic. Therefore, the presence of the warm Gulf Stream anomaly in the driest members likely facilitated the amplification of a "stationary wave train" propagating across the Atlantic. Following the 8 driest members, this wave train likely favoured the formation of a persistent anticyclonic ridge over the European continent, effectively shielding it from Atlantic storms. A similar significant warm configuration is observed in the 2018 and 2022 significance maps (Fig. 4.17c-d), where stippling cover parts of Atlantic belonging to the Gulf Stream path, indicating a possible analogy with the Rossby wave mechanism just described for 2015. The fact that this warm anomaly was already pronounced in May 2018 and 2022 (Fig. 4.16c-d) might have influenced the model towards a correct forecast, thereby identifying it as a potential source of predictability.

Notably, the eight driest members for 2022 significantly predicted all of the triggering factors identified in this analysis: a warm Mediterranean and Northeast Atlantic, a cold blob over the subpolar region, and anomalous warming along the US coast. The compounding of these multiple oceanic drivers is highly consistent with the SEAS5 model's overestimation of the 2022 summer drought's severity.

Chapter 5

Discussion

This analysis shows that the fifth generation of ECMWF seasonal forecast model showed low accuracy in forecasting the European summer droughts of 2003 and 2015 and better skill for those of 2018 and 2022, as measured by the Brier Score. In light of this, we sought for common climate patterns between poorly predicted and well-predicted summers.

A notable feature in the performance time series of the model is the abrupt drop in the BS time series observed from 2017 onwards (Fig. 4.2), coinciding with the accurately predicted droughts of 2018 and 2022. While this could be partially attributed to the atmospheric dynamics of those specific years (e.g., strong positive SNAO forcing), this shift aligns with the transition from the SEAS5 historical hindcast dataset to the real-time operational forecast dataset. This discrepancy can be explained by the statistical impact of the ensemble size on the final forecasts. Indeed, a fundamental factor contributing to the observed skill discrepancy is the direct mathematical relationship between ensemble size and probabilistic forecast accuracy (Richardson, 2001). Metrics such as the BS, which evaluates the reliability and resolution of probabilistic predictions, are highly sensitive to the number of members comprising the ensemble (Richardson, 2001; Wilks, 2011). During the hindcast period (spanning up to 2016 and encompassing the 2003 and 2015 case studies), the SEAS5 system is limited to a 25-member ensemble. In contrast, the operational forecast period (from 2017 onwards, including the 2018 and 2022 events) utilizes a significantly expanded 51-member ensemble (Johnson et al., 2019).

This difference in ensemble size can alter the model's ability to forecast extreme climatic anomalies, such as severe droughts. When forecasting such extreme events, a crucial distinction must be made between the deterministic ensemble mean and the probabilistic distribution. While a larger ensemble typically smooths the deterministic mean state, it fundamentally improves the probabilistic detection of rare events. Extreme atmospheric patterns—such as the persistent blocking required for a severe drought—reside in the far "tails" of the Probability Density Function. A smaller 25-member ensemble (2003, 2015) explores a narrower range of chaotic atmospheric trajectories. Consequently, it systematically under-samples these statistical tails, often failing entirely to simulate the specific, rare dynamic combination needed for the extreme event. This results in the model assigning a near-zero probability to the drought, which severely penalizes probabilistic metrics like the BS when the event actually occurs. Conversely, the expanded 51-member ensemble provides a significantly denser sampling of the atmospheric phases. By generating twice as many possible future scenarios, the model is statistically more capable of populating the tails of the distribution and successfully captures the minority of members that develop extreme blocking patterns. This robust sampling translates into a higher, non-zero probabilistic signal for the extreme event, possibly improving the BS during the operational forecast period (2018, 2022) independently of the underlying meteorological forcing.

Beyond the ensemble size, the data used to initialize the model introduces a structural inhomogeneity between the hindcasts (2003, 2015) and the forecasts (2018, 2022). As mentioned in Section 2.2, the hindcasts (1981–2016) are initialized using historical atmospheric and oceanic reanalyses, which are retrospectively stabilized datasets. Conversely, operational forecasts (2017–2022) are initialized using real-time Operational Analyses. Transitioning between these distinct datasets can introduce subtle initial-state biases (Johnson et al., 2019).

Furthermore, the role of the climatological baseline is crucial in explaining the recent improvement in model skill. In this study, the SWBA was computed against the 1993-2016 reference climatology, and so the characterization of drought severity. Because of the accelerating global warming trend, the operational years (2018 and 2022) are subjected to a significantly warmer background state compared to this historical average. Consequently, the model is initialized in a warmer climate and

naturally drifts towards predicting positive temperature and negative water balance anomalies as a default state relative to the 1993-2016 baseline. When a drought physically occurs in these recent years, the model captures it with high confidence because the anthropogenic warming trend has already preconditioned the forecasts towards a warm and dry anomaly (Weisheimer et al., 2017), while in 2003 for instance it was much more difficult to foresee such extreme temperatures. One way to limit this effect are detrending data (as done in this study for the SWBA computation).

The significance test conducted on the driest and wettest mambers of the model for temperature and rainfall anomalies suggests a tendency towards drought predictions when higher than average temperatures and lower than average rainfall were expected, consistently with the SWBA structure, being a stanzardised anomaly of P – PET at a given location. The same is true for the model's ensemble mean, which showed positive anomalies values of t2m and negative anomalies values of tp for well-predicted summers, and the opposite for poorly predicted summers.

The results from the MSLP analysis highlights that the model struggles to forecast blocking patterns, especially if they occur during a negative SNAO phase. In general, a positive SNAO configuration forces a northward displacement of the Atlantic jet stream and the associated storm track, causing drier and warmer summers over northwest Europe, especially United Kingdom and part of Scandinavia, and more weakly, wetter and cooler conditions over southern Europe and Eastern Mediterranean (Folland et al., 2009). This kind of configuration is very similar to observations in the summers of 2018 and 2022, where SEAS5 more accurately predicted the drought events and their respective atmospheric configurations.

A critical discrepancy emerges when analysing the synoptic configuration of the poorly predicted drought years, 2003 and 2015. Reanalysis data revealed that both events were characterized by a negative phase of the SNAO, featuring high pressure over the Greenland and Arctic sector. The SEAS5 ensemble mean failed to reproduce the observed 2003 and 2015 blocking-like anomalous atmospheric circulation occurring during the negative SNAO. In particular, although the 2003 summer was mathematically classified as a negative SNAO phase, the observed synoptic configuration was characterized by a dipolar structure (Fig. 4.12a) that does not fit the standard SNAO circulation described by Folland et al. (2009).

During the 2015 summer, the atmospheric circulation formed a sharp West-East dipole between a low-pressure system anchored over the UK (the negative pole of the SNAO) and a persistent high-pressure ridge developed over Central-Eastern Europe (red area in Fig. 4.12b), which induced intense warm air advection from the Mediterranean and North Africa towards Central Europe (Duchez et al., 2016). Therefore, while the wet weather in the northwest part of the continent is typical of the negative SNAO, the drought occurred in the central-eastern sector.

The SNAO analysis revealed that the model systematically associates the negative phase of the SNAO with cool, wet, or average conditions across the European continent, while issuing sharper drought forecasts primarily during positive SNAO phases. This behaviour indicates a dynamical inability of the model to resolve a blocking configuration during a negative SNAO phase, a limitation that was particularly evident during the observed events of 2003 and 2015. This deficiency is empirically demonstrated by the distribution of the ensemble members: those that successfully predicted the drought conditions (driest members) consistently exhibited positive SNAO values across all four analysed summers, whereas the members with the poorest performance (wettest members) showed negative SNAO values (Tab. 5). Furthermore, the 2003 case study provides critical evidence that the model struggles to associate a negative SNAO phase with significant warm anomalies in the Mediterranean region. Although the ensemble mean correctly anticipated a negative SNAO signal for that year, it failed to capture the heat extreme, predicting instead near-normal conditions for the Mediterranean basin. This decoupling aligns with the climatological characterization by Folland et al. (2009), who established that the SNAO exerts a dominant influence on the hydroclimate of Northern Europe, while its impacts on Southern Europe and the Mediterranean sector is significantly weaker.

Overall, our results suggest that while SEAS5 has high skill in predicting droughts driven by positive SNAO phases (2018, 2022)—during which the storm trackshifts northward—it struggles to capture exceptional drought events driven by atmospheric blockings that occur under negative SNAO conditions. In practice, the model struggles to predict blocking phenomena, but intuitively manages to predict dry conditions in Europe when these are associated with a positive SNAO phase which is typically linked with dry condition over the central and northern

part of the continent. In this sense, we would expect a greater performance of the SEAS5 model in the prediction of summer European droughts in the years characterized by a positive SNAO phase. Additionally, the prior-to-summer SNAO might represent a source of summer droughts predictability, as 2018 and 2022 showed a strong positive SNAO signal already in May. Essentially, if a negative SNAO is recorded before the summer, one should question the accuracy of the summer seasonal forecasts for the following summer.

Predicting the correct SNAO phase represents a significant challenge in seasonal climatology, as summer atmospheric variability is inherently weaker and less persistent than its winter counterpart (Folland et al., 2009). However, recent advancements in dynamic modelling have demonstrated that the SNAO is a predictable component of the climate system on seasonal timescales. Specifically, Dunstone et al. (2016) provided evidence that high-resolution systems can achieve skilful predictions of the SNAO. Furthermore, the newest climate models include more detailed orography than SEAS5, which would help resolve atmospheric blocking phenomena typical of a drought event.

Current operational forecasting relies primarily on coupled Atmosphere-Ocean General Circulation Models, such as the ECMWF SEAS5 and the Met Office GloSea5 systems, which derive predictability from slowly evolving boundary conditions like SST. In this context, the ENSO teleconnection pattern plays a crucial modulating role. According to the linear relationship described by Folland et al. (2009), tropical Pacific variability influences the North Atlantic circulation, where an El Niño event is statistically associated with a positive phase of the SNAO. This teleconnection is particularly relevant for interpreting the model's behaviour during the 2015 event. The summer of 2015 coincided with the onset of a very strong El Niño event in the Pacific. Based on the assumption of linearity suggested by Folland et al. (2009), this strong tropical forcing would physically predispose the atmospheric circulation towards a positive SNAO phase. Consequently, it is plausible to hypothesize that the SEAS5 model's forecast for 2015 was influenced by this concurrent El Niño signal: the latter appeared biased to predict a positive SNAO pattern, creating a conflict with local North Atlantic drivers that ultimately resulted in the observed negative SNAO configuration.

In addition to MSLP, drought forecasts in Europe also appeared to be influenced

by certain global oceanic and atmospheric circulation patterns. In particular, previous studies indicate a statistically significant relationship between the forecast of a cold anomaly in the subpolar North Atlantic and a dry summer in Europe (Duchez et al. in 2016). This connection, widely discussed for observations of the 2015 drought, is also represented in the driest members of 2003, 2018 and 2022 forecasts, and it was already recorded 1 month prior to the well-predicted summers, making it a possible source of drought predictability. Particularly, the model seems to foresee dry conditions over Europe when a strong inter-gyre SST gradient between subpolar cold anomalies and warm Gulf Stream appears.

Another significant oceanic pattern which could influence droughts predictability is the warm SST along the US East Cost itself, along the Gulf Stream path. This condition has been observed with significance in the driest members of 2015 and 2022 (Fig. 4.17b-d), as well as in the May observations maps of the well-predicted summers (Fig. 4.16c-d). Our analysis further suggests a possible correlation between the warm Gulf Stream and the prediction of a positive SNAO. Indeed, the driest members of the ensemble which predict significantly warm SST anomalies in the Gulf Stream are the same which, according to Tab. 4.1, predict a positive SNAO phase, regardless of the year.

We found no statistical evidences of ENSO influencing European summer drought prediction. However, the significance test highlights those distinctive features of the driest or wettest members: if all members of the ensemble predicted the same outcome, that particular pattern that may have influenced the model's prediction would not appear to be statistically significant. For this reason, we cannot even conclude that the positive phase of the ENSO predicted by SEAS5 for 2015 had no impact on the seasonal forecasts. The same applies to the correct model's prediction of a strong negative ENSO phase in 2022. To verify whether all members agreed on this SST forecast, it is necessary to check the anomalies predicted by each member to see the overall trend of the model forecasts. For instance, the ensemble model correctly predicts the negative ENSO phase for summer 2022, but it did not appear to be significant in the analysis. However, according to Patterson et al. (2024), the 2022 jet shift observed in the model outcomes was likely resulted from the combination between the real forcing from La Niña and the model's inherent tendency to shift the jet poleward under warming scenarios.

The coexistence between these two factors might have contributed to enhance the accuracy of summer 2022 forecast.

The last significant SST pattern common to the driest members for all four summers is the warm Mediterranean and Northeast Atlantic - off the coasts of Europe. This suggests that these SST anomalies affect atmospheric conditions over land, fostering the development of drought, here evaluated as an anomaly in P - PET.

Observed SST anomalies prior to summer for the poorly predicted summers of 2003 and 2015 lack a strong signal from all the patterns just described (Fig. 4.16a-b), while they are present in those for the well-predicted summers of 2018 and 2022 (Fig. 4.16c-d). The only exception is the absence of the cold blob in 2022, even if the driest members still predicted it, reinforcing our conclusion that the cold blob is a potential source of predictability.

Additionally, to fully understand the dynamical inabilities of the SEAS5 model—particularly its failure to resolve complex atmospheric blocking during specific SNAO phases—the inclusion of two additional climatic variables as Geopotential Height at 500 hPa (Z500) and Zonal Wind at 300 hPa (U300) would improve the robustness of this performance evaluation. While the variables here analysed provide a robust foundation for evaluating the surface expression and oceanic boundary forcings of summer droughts, a comprehensive physical diagnosis of the model's performance would also require the evaluation of the vertical structure of the troposphere and the land-surface state. In details, Z500 represents the mid-tropospheric circulation. While MSLP illustrates the surface framework of the weather systems, Z500 is the primary variable used to identify planetary Rossby waves and deep atmospheric blocking structures, such as Omega blocks. Integrating Z500 into the accuracy analysis would clarify whether the model's failure to predict the 2003 or 2015 extreme droughts was due to an inability to simulate the large-scale mid-level ridge itself, or merely a failure to accurately translate a correctly predicted ridge into surface temperature and precipitation anomalies.

Furthermore, U300 defines the position, strength, and waviness of the Jet Stream. The surface SNAO index is intrinsically linked to the behaviour of this upper-level jet. By analysing U300, it is possible to empirically quantify the model's inability highlighted during the 2003 and 2015 events.

In the end, expanding the analytical framework to others seasonal models would bring further improvements for the evaluation of seasonal forecasts performance regarding European summer droughts. A comparative multi-model analysis would allow to investigate whether there are systemic analogies in forecast failures across different modelling centres. Crucially, it would help determine if the dynamical inability to accurately resolve atmospheric blocking and decouple the negative phase of the SNAO from strictly cool and wet conditions is an internal bias of the SEAS5 architecture, or a generalized limitation shared by the current generation of coupled atmosphere-ocean seasonal models.

Chapter 6

Conclusion

This thesis investigated the sources of predictability of summer droughts in Europe, utilizing reanalysis, observational data, and seasonal forecasts from the ECMWF SEAS5 model.

The observed negative trend in the European summer water balance underscores a progressive drying of the continent, driven primarily by rising temperatures and increased atmospheric evaporative demand, confirming previous findings (Stagge et al., 2017; Christidis et al., 2021). The evaluation of the SEAS5 model's performance revealed significant variability in its ability to predict extreme summer droughts.

In particular, this analysis demonstrated the model's poor skill in forecasting the severe summer droughts of 2003 and 2015, while showing good skill for the events of 2018 and 2022. Our analysis suggests that this discrepancy might be tied to the model's handling of large-scale atmospheric and oceanic circulation patterns, particularly of the SNAO. Indeed, the seasonal model tends to successfully predict those droughts associated with the positive SNAO phase (e.g., 2018, 2022), while struggles when confronted with the negative (e.g., 2003, 2015). While reanalysis data show that a negative SNAO can still lead to severe droughts driven by complex atmospheric blocking (as seen in 2003 and 2015), the SEAS5 model tends to uniformly associate a negative SNAO with cooler and wetter conditions across the continent. This indicates a fundamental dynamical limitation in the model's ability to resolve complex blocking high-pressure systems, particularly those occurring over Europe under negative SNAO forcing.

Another key finding of this study is that oceanic patterns play a crucial role in drought predictability. The analysis identified statistically significant relationships between accurate drought forecasts and specific SST anomalies. Notably, a cold SST anomaly in the subpolar North Atlantic and a warm anomaly along the Gulf Stream path were identified as statistically significant precursors in the model's successful drought predictions, likely due to their influence on European summer climate and on the SNAO pattern. Furthermore, a warm Mediterranean and Northeast Atlantic anomaly was a statistical consistent feature in the most accurate ensemble members across all analysed summers.

In this regard, the observed prior-to-summer SNAO, as well as the oceanic pattern here mentioned, could be considered as sources of predictability, serving as indicators of the SEAS5 summer forecasts uncertainty.

Last, further research investigating the sources of predictability of European summer droughts remains necessary and of great importance. Specifically, understanding the climatological patterns which influence the seasonal models' reliability allows end-users and decision-makers to critically interpret model outputs. Simultaneously, identifying these predictability drivers provides essential feedback to correct systematic biases and refine the architecture of the seasonal models themselves.

References

AghaKouchak, A., Chiang, F., Huning, L. S., Love, C. A., Mallakpour, I., Mazdiyasni, O., Moftakhari, H., Papalexiou, S. M., Ragno, E., & Sadegh, M. (2020). Climate Extremes and Compound Hazards in a Warming World. Annual Review of Earth and Planetary Sciences, 48(1), 519–548. https://doi.org/10.1146/annurev-earth-071719-055228

Allen, R. G., Pereira, L. S., Raes, D., & Smith, M. (1998). FAO Irrigation and drainage paper No. 56. Food and Agriculture Organization of the United Nations, 56(97), e156.

Avanzi, F., Munerol, F., Milelli, M., Gabellani, S., Massari, C., Girotto, M., Cremonese, E., Galvagno, M., Bruno, G., Morra Di Cella, U., Rossi, L., Altamura, M., & Ferraris, L. (2024). Winter snow deficit was a harbinger of summer 2022 socio-hydrologic drought in the Po Basin, Italy. Communications Earth & Environment, 5(1), 64. https://doi.org/10.1038/s43247-024-01222-z

Beguería, S., Vicente-Serrano, S. M., Reig, F., & Latorre, B. (2014). Standardized precipitation evapotranspiration index (SPEI) revisited: Parameter fitting, evapotranspiration models, tools, datasets and drought monitoring. International Journal of Climatology, 34(10), 3001–3023. https://doi.org/10.1002/joc.3887

Beobide-Arsuaga, G., Düsterhus, A., Müller, W. A., Barnes, E. A., & Baehr, J. (2023). Spring Regional Sea Surface Temperatures as a Precursor of European Summer Heatwaves. Geophysical Research Letters, 50(2), e2022GL100727. https://doi.org/10.1029/2022GL100727

Black, E., Blackburn, M., Harrison, G., Hoskins, B., & Methven, J. (2004). Factors contributing to the summer 2003 European heatwave. Weather, 59(8), 217–223.

Bladé, I., Fortuny, D., Van Oldenborgh, G. J., & Liebmann, B. (2012). The summer North Atlantic Oscillation in CMIP3 models and related uncertainties in projected summer drying in Europe. Journal of Geophysical Research: Atmospheres, 117(D16), 2012JD017816. https://doi.org/10.1029/2012JD017816

Calì Quaglia, F., Terzago, S., & Von Hardenberg, J. (2022). Temperature and precipitation seasonal forecasts over the Mediterranean region: Added value compared to simple forecasting methods. Climate Dynamics, 58(7–8), 2167–2191. https://doi.org/10.1007/s00382-021-05895-6

Cerato, G., Bellomo, K., & von Hardenberg, J. (2025). Summer drought predictability in the Euro-Mediterranean region in seasonal forecasts. Journal of Hydrometeorology, 26(12), 1939–1956. https://doi.org/10.1175/JHM-D-25-0039.1

Cheval, S., Busuioc, A., Dumitrescu, A., & Birsan, M.-V. (2014). Spatiotemporal variability of meteorological drought in Romania using the standardized precipitation index (SPI). Climate Research, 60, 235–248. https://doi.org/10.3354/cr01245

Christidis, N., & Stott, P. A. (2021). The influence of anthropogenic climate change on wet and dry summers in Europe. Science Bulletin, 66(8), 813–823. https://doi.org/10.1016/j.scib.2021.01.020

Cohen, J., Screen, J. A., Furtado, J. C., Barlow, M., Whittleston, D., Coumou, D., Francis, J., Dethloff, K., Entekhabi, D., Overland, J., & Jones, J. (2014). Recent Arctic amplification and extreme mid-latitude weather. Nature Geoscience, 7(9), 627–637. https://doi.org/10.1038/ngeo2234

Copernicus Climate Change Service. (2018). ERA5 hourly data on single levels from 1940 to present. Copernicus Climate Change Service (C3S) Climate Data Store (CDS). https://doi.org/10.24381/CDS.ADBB2D47

Copernicus Climate Change Service. (2023). European State of the Climate 2022. https://climate.copernicus.eu/esotc/2022

Coumou, D., Di Capua, G., Vavrus, S., Wang, L., & Wang, S. (2018). The influence of Arctic amplification on mid-latitude summer circulation. Nature Communications, 9(1), 2959. https://doi.org/10.1038/s41467-018-05256-8

Crausbay, S. D., Ramirez, A. R., Carter, S. L., Cross, M. S., Hall, K. R., Bathke, D. J., Betancourt, J. L., Colt, S., Cravens, A. E., & Dalton, M. S. (2017). Defining ecological drought for the twenty-first century. Bulletin of the American Meteorological Society, 98(12), 2543–2550. https://doi.org/10.1175/BAMS-D-16-0292.1

Cresswell-Clay, N., Ummenhofer, C. C., Thatcher, D. L., Wanamaker, A. D., Denniston, R. F., Asmerom, Y., & Polyak, V. J. (2022). Twentieth-century Azores High expansion unprecedented in the past 1,200 years. Nature Geoscience, 15(7), 548–553. https://doi.org/10.1038/s41561-022-00971-w

Dai, A. (2011). Drought under global warming: A review. WIREs Climate Change, 2(1), 45–65. https://doi.org/10.1002/wcc.81

Dai, A. (2013). Increasing drought under global warming in observations and models. Nature Climate Change, 3(1), 52–58. https://doi.org/10.1038/nclimate1633

Dobesch, H., Dumolard, P., & Dyras, I. (2013). Spatial interpolation for climate data: The use of GIS in climatology and meteorology. John Wiley & Sons.

Duchez, A., Frajka-Williams, E., Josey, S. A., Evans, D. G., Grist, J. P., Marsh, R., McCarthy, G. D., Sinha, B., Berry, D. I., & Hirschi, J. J. (2016). Drivers of exceptionally cold North Atlantic Ocean temperatures and their link to the 2015 European heat wave. Environmental Research Letters, 11(7), 074004. https://doi.org/10.1088/1748-9326/11/7/074004

Dunstone, N., Smith, D. M., Hardiman, S. C., Hermanson, L., Ineson, S., Kay, G., Li, C., Lockwood, J. F., Scaife, A. A., Thornton, H., Ting, M., & Wang, L. (2023). Skilful predictions of the Summer North Atlantic Oscillation. Communications Earth & Environment, 4(1), 409. https://doi.org/10.1038/s43247-023-01063-2

ECMWF. (2018, January 17). ECMWF's new long-range forecasting system

SEAS5. https://www.ecmwf.int/en/newsletter/154/meteorology/ecmwfs-new-long-range-forecasting-system-seas5

ECMWF. (2026, January 5). ERA5: Data documentation. https://confluence.ecmwf.int/display/CKB/ERA5%3A+data+documentation#ERA5:datadocum Observations

European Environment Agency. (2025, October 14). Economic losses from weather- and climate-related extremes in Europe. https://www.eea.europa.eu/en/analysis/indicators/economic-losses-from-climate-related

Feudale, L., & Shukla, J. (2011). Influence of sea surface temperature on the European heat wave of 2003 summer. Part I: An observational study. Climate Dynamics, 36(9–10), 1691–1703. https://doi.org/10.1007/s00382-010-0788-0

Fink, A. H., Brücher, T., Krüger, A., Leckebusch, G. C., Pinto, J. G., & Ulbrich, U. (2004). The 2003 European summer heatwaves and drought-synoptic diagnosis and impacts. Weather, 59(8), 209–216. https://doi.org/10.1256/wea.73.04

Fischer, E. M., Seneviratne, S. I., Lüthi, D., & Schär, C. (2007). Contribution of land-atmosphere coupling to recent European summer heat waves. Geophysical Research Letters, 34(6), 2006GL029068. https://doi.org/10.1029/2006GL029068

Folland, C. K., Knight, J., Linderholm, H. W., Fereday, D., Ineson, S., & Hurrell, J. W. (2009). The Summer North Atlantic Oscillation: Past, Present, and Future. Journal of Climate, 22(5), 1082–1103. https://doi.org/10.1175/2008JCLI2459.1

Frierson, D. M. W., Lu, J., & Chen, G. (2007). Width of the Hadley cell in simple and comprehensive general circulation models. Geophysical Research Letters, 34(18), 2007GL031115. https://doi.org/10.1029/2007GL031115

García-Herrera, R., Díaz, J., Trigo, R. M., Luterbacher, J., & Fischer, E. M. (2010). A Review of the European Summer Heat Wave of 2003. Critical Reviews in Environmental Science and Technology, 40(4), 267–306. https://doi.org/10.1080/10643380802238137

Garrido-Perez, J. M., Vicente-Serrano, S. M., Barriopedro, D., García-Herrera, R., Trigo, R., & Beguería, S. (2024). Examining the outstanding Euro-Mediterranean drought of 2021–2022 and its historical context. Journal of Hydrology, 630, 130653. https://doi.org/10.1016/j.jhydrol.2024.130653

Gulev, S. K., Thorne, P. W., Ahn, J., Dentener, F. J., Domingues, C. M., Gerland, S., Gong, D., Kaufman, D. S., Nnamchi, H. C., & Quaas, J. (2021). Changing state of the climate system. Climate Change 2021: The Physical Science Basis. Contribution of Working Group I to the Sixth Assessment Report of the Intergovernmental Panel on Climate Change, 287–422. https://doi.org/10.1017/9781009157896.004

Hanel, M., Rakovec, O., Markonis, Y., Máca, P., Samaniego, L., Kysel, J., & Kumar, R. (2018). Revisiting the recent European droughts from a long-term perspective. Scientific Reports, 8(1), 9499. https://doi.org/10.1038/s41598-018-27464-4

Hersbach, H., Bell, B., Berrisford, P., Hirahara, S., Horányi, A., Muñoz-Sabater, J., Nicolas, J., Peubey, C., Radu, R., Schepers, D., Simmons, A., Soci, C., Abdalla, S., Abellan, X., Balsamo, G., Bechtold, P., Biavati, G., Bidlot, J., Bonavita, M., ... Thépaut, J. (2020). The ERA5 global reanalysis. Quarterly Journal of the Royal Meteorological Society, 146(730), 1999–2049. https://doi.org/10.1002/qj.3803

Hurrell, J. W. (1995). Decadal Trends in the North Atlantic Oscillation: Regional Temperatures and Precipitation. Science, 269(5224), 676–679. https://doi.org/10.1126/science.269.5224.676

Hurrell, J. W., Kushnir, Y., Ottersen, G., & Visbeck, M. (2003). An overview of the North Atlantic Oscillation. In J. W. Hurrell, Y. Kushnir, G. Ottersen, & M. Visbeck (Eds), Geophysical Monograph Series (Vol. 134, pp. 1–35). American Geophysical Union. https://doi.org/10.1029/134GM01

Intergovernmental Panel on Climate Change (IPCC). (2023). Climate Change 2022 – Impacts, Adaptation and Vulnerability: Working Group II Contribution to the Sixth Assessment Report of the Intergovernmental Panel on Climate Change (1st edn). Cambridge University Press. https://doi.org/10.1017/9781009325844

Ionita, M., Tallaksen, L. M., Kingston, D. G., Stagge, J. H., Laaha, G., Van Lanen,

H. A., Scholz, P., Chelcea, S. M., & Haslinger, K. (2017). The European 2015 drought from a climatological perspective. Hydrology and Earth System Sciences, 21(3), 1397–1419. https://doi.org/10.5194/hess-21-1397-2017

Jiao, T., Williams, C. A., De Kauwe, M. G., Schwalm, C. R., & Medlyn, B. E. (2021). Patterns of post-drought recovery are strongly influenced by drought duration, frequency, post-drought wetness, and bioclimatic setting. Global Change Biology, 27(19), 4630–4643. https://doi.org/10.1111/gcb.15788

Johnson, S. J., Stockdale, T. N., Ferranti, L., Balmaseda, M. A., Molteni, F., Magnusson, L., Tietsche, S., Decremer, D., Weisheimer, A., & Balsamo, G. (2019). SEAS5: The new ECMWF seasonal forecast system. Geoscientific Model Development, 12(3), 1087–1117. https://doi.org/10.5194/gmd-12-1087-2019

Keyantash, J., & Dracup, J. A. (2002). The quantification of drought: An evaluation of drought indices. Bulletin of the American Meteorological Society, 83(8), 1167–1180. https://doi.org/10.1175/1520-0477-83.8.1167

Knapp, A. K., Beier, C., Briske, D. D., Classen, A. T., Luo, Y., Reichstein, M., Smith, M. D., Smith, S. D., Bell, J. E., & Fay, P. A. (2008). Consequences of more extreme precipitation regimes for terrestrial ecosystems. Bioscience, 58(9), 811–821. https://doi.org/10.1641/B580908

Krishnamurthy, V. (2019). Predictability of Weather and Climate. Earth and Space Science, 6(7), 1043–1056. https://doi.org/10.1029/2019EA000586

Lindsey, R., & Dahlman, L. (2020). Climate change: Global temperature. Climate. Gov, 16, 1–5.

Lionello, P., Malanotte-Rizzoli, P., Boscolo, R., Alpert, P., Artale, V., Li, L., Luterbacher, J., May, W., Trigo, R., & Tsimplis, M. (2006). The Mediterranean climate: An overview of the main characteristics and issues. In Developments in earth and environmental sciences (Vol. 4, pp. 1–26). Elsevier. https://www.sciencedirect.com/science/article/pii/S1571919706800030

Lu, J., Vecchi, G. A., & Reichler, T. (2007). Expansion of the Hadley cell

under global warming. Geophysical Research Letters, 34(6), 2006GL028443. https://doi.org/10.1029/2006GL028443

McKee, T. B., Doesken, N. J., & Kleist, J. (1993). The relationship of drought frequency and duration to time scales. Proceedings of the 8th Conference on Applied Climatology, 17(22), 179–183. https://climate.colostate.edu/pdfs/relationshipofdroughtfrequency.pdf

McPhaden, M. J., Zebiak, S. E., & Glantz, M. H. (2006). ENSO as an Integrating Concept in Earth Science. Science, 314(5806), 1740–1745. https://doi.org/10.1126/science.1132588

Mecking, J. V., Drijfhout, S. S., Hirschi, J. J.-M., & Blaker, A. T. (2019). Ocean and atmosphere influence on the 2015 European heatwave. Environmental Research Letters, 14(11), 114035. https://doi.org/10.1088/1748-9326/ab4d33

Minobe, S., Kuwano-Yoshida, A., Komori, N., Xie, S.-P., & Small, R. J. (2008). Influence of the Gulf Stream on the troposphere. Nature, 452(7184), 206–209. https://doi.org/10.1038/nature06690

Miralles, D. G., Teuling, A. J., Van Heerwaarden, C. C., & Vilà-Guerau De Arellano, J. (2014). Mega-heatwave temperatures due to combined soil desiccation and atmospheric heat accumulation. Nature Geoscience, 7(5), 345–349. https://doi.org/10.1038/ngeo2141

Miralles, D. G., Gentine, P., Seneviratne, S. I., & Teuling, A. J. (2019). Land–atmospheric feedbacks during droughts and heatwaves: State of the science and current challenges. Annals of the New York Academy of Sciences, 1436(1), 19–35. https://doi.org/10.1111/nyas.13912

Molteni, F., Buizza, R., Palmer, T. N., & Petroliagis, T. (1996). The ECMWF Ensemble Prediction System: Methodology and validation. Quarterly Journal of the Royal Meteorological Society, 122(529), 73–119. https://doi.org/10.1002/qj.49712252905

National Centre for Atmospheric Research. (2025). The climate data guide: SST

data: HadISST v1.1. https://climatedataguide.ucar.edu/climate-data/sst-data-hadisst-v11

Ossó, A., Sutton, R., Shaffrey, L., & Dong, B. (2018). Observational evidence of European summer weather patterns predictable from spring. Proceedings of the National Academy of Sciences, 115(1), 59–63. https://doi.org/10.1073/pnas.1713146114

Patterson, M., Befort, D. J., O'Reilly, C. H., & Weisheimer, A. (2024). Drivers of the ECMWF SEAS5 seasonal forecast for the hot and dry European summer of 2022. Quarterly Journal of the Royal Meteorological Society, 150(765), 4969–4986. https://doi.org/10.1002/qj.4851

Rayner, N. A., Parker, D. E., Horton, E. B., Folland, C. K., Alexander, L. V., Rowell, D. P., Kent, E. C., & Kaplan, A. (2003). Global analyses of sea surface temperature, sea ice, and night marine air temperature since the late nineteenth century. Journal of Geophysical Research: Atmospheres, 108(D14), 2002JD002670. https://doi.org/10.1029/2002JD002670

Richardson, D. S. (2001). Measures of skill and value of ensemble prediction systems, their interrelationship and the effect of ensemble size. Quarterly Journal of the Royal Meteorological Society, 127(577), 2473–2489. https://doi.org/10.1002/qj.49712757715

Rousi, E., Fink, A. H., Andersen, L. S., Becker, F. N., Beobide-Arsuaga, G., Breil, M., Cozzi, G., Heinke, J., Jach, L., Niermann, D., Petrovic, D., Richling, A., Riebold, J., Steidl, S., Suarez-Gutierrez, L., Tradowsky, J. S., Coumou, D., Düsterhus, A., Ellsäßer, F., ... Xoplaki, E. (2023). The extremely hot and dry 2018 summer in central and northern Europe from a multi-faceted weather and climate perspective. Natural Hazards and Earth System Sciences, 23(5), 1699–1718. https://doi.org/10.5194/nhess-23-1699-2023

Screen, J. A. (2013). Influence of Arctic sea ice on European summer precipitation. Environmental Research Letters, 8(4), 044015. https://doi.org/10.1088/1748-9326/8/4/044015

Seneviratne, S. I., Corti, T., Davin, E. L., Hirschi, M., Jaeger, E. B., Lehner, I., Orlowsky, B., & Teuling, A. J. (2010). Investigating soil moisture–climate interactions in a changing climate: A review. Earth-Science Reviews, 99(3–4), 125–161. https://doi.org/10.1016/j.earscirev.2010.02.004

Setchell, H. (2022, July 21). ECMWF. https://www.ecmwf.int/en/about

Slingo, J., & Palmer, T. (2011). Uncertainty in weather and climate prediction. Philosophical Transactions of the Royal Society A: Mathematical, Physical and Engineering Sciences, 369(1956), 4751–4767. https://doi.org/10.1098/rsta.2011.0161

Sousa, P. M., Barriopedro, D., Ramos, A. M., García-Herrera, R., Espírito-Santo, F., & Trigo, R. M. (2019). Saharan air intrusions as a relevant mechanism for Iberian heatwaves: The record breaking events of August 2018 and June 2019. Weather and Climate Extremes, 26, 100224. https://doi.org/10.1016/j.wace.2019.100224

Spinoni, J., Vogt, J. V., Naumann, G., Barbosa, P., & Dosio, A. (2018). Will drought events become more frequent and severe in Europe? International Journal of Climatology, 38(4), 1718–1736. https://doi.org/10.1002/joc.5291

Stagge, J. H., Kingston, D. G., Tallaksen, L. M., & Hannah, D. M. (2017). Observed drought indices show increasing divergence across Europe. Scientific Reports, 7(1), 14045. https://doi.org/10.1038/s41598-017-14283-2

Stockdale, T. (2021). SEAS5 user guide. https://doi.org/10.21957/2Y67999Y

Stott, P. A., Stone, D. A., & Allen, M. R. (2004). Human contribution to the European heatwave of 2003. Nature, 432(7017), 610–614. https://doi.org/10.1038/nature03089

Sutton, R. T., & Dong, B. (2012). Atlantic Ocean influence on a shift in European climate in the 1990s. Nature Geoscience, 5(11), 788–792. https://doi.org/10.1038/ngeo1595

Svoboda, M. D., & Fuchs, B. A. (2016). Handbook of drought indicators and indices (Vol. 2). World Meteorological Organization Geneva, Switzerland.

Tannehill, I. R. (1947). Drought, its causes and effects (Vol. 64). LWW.

Thornthwaite, C. W. (1948). An approach toward a rational classification of climate. Geographical Review, 38(1), 55–94.

Trigo, R. M., Barriopedro, D., Garrido-Perez, J. M., Simon, A., Plecha, S. M., Teles-Machado, A., Russo, A., & Garcia-Herrera, R. (2025). The outstanding European and Mediterranean heatwave activity during summer 2022. Atmospheric Research, 323, 108195. https://doi.org/10.1016/j.atmosres.2025.108195

Troccoli, A. (2010). Seasonal climate forecasting: A review. Meteorological Applications, 17(3), 251–268. https://doi.org/10.1002/met.184

Van Loon, A. F., & Laaha, G. (2015). Hydrological drought severity explained by climate and catchment characteristics. Journal of Hydrology, 526, 3–14. https://doi.org/10.1016/j.jhydrol.2014.10.059

Vicente-Serrano, S. M., Beguería, S., & López-Moreno, J. I. (2010). A multiscalar drought index sensitive to global warming: The standardized precipitation evapotranspiration index. Journal of Climate, 23(7), 1696–1718. https://doi.org/10.1175/2009JCLI2909.1

Vicente-Serrano, S. M., Lopez-Moreno, J.-I., Beguería, S., Lorenzo-Lacruz, J., Sanchez-Lorenzo, A., García-Ruiz, J. M., Azorin-Molina, C., Morán-Tejeda, E., Revuelto, J., & Trigo, R. (2014). Evidence of increasing drought severity caused by temperature rise in southern Europe. Environmental Research Letters, 9(4), 044001. https://doi.org/10.1088/1748-9326/9/4/044001

Weisheimer, A., Schaller, N., O'Reilly, C., MacLeod, D. A., & Palmer, T. (2017). Atmospheric seasonal forecasts of the twentieth century: Multi-decadal variability in predictive skill of the winter North Atlantic Oscillation (NAO) and their potential value for extreme event attribution. Quarterly Journal of the Royal Meteorological Society, 143(703), 917–926. https://doi.org/10.1002/qj.2976

Wilhite, D. A., & Glantz, M. H. (1985). Understanding: The Drought Phenomenon: The Role of Definitions. Water International, 10(3), 111–120.

https://doi.org/10.1080/02508068508686328

Wilhite, D. A., & Svoboda, M. D. (2000). Drought early warning systems in the context of drought preparedness and mitigation. In D. A. Wilhite (Ed.), Early warning systems for drought preparedness and drought management (pp. 1–21). World Meteorological Organization.

Wilks, D. S. (2011). Statistical methods in the atmospheric sciences (Vol. 100). Academic press.

Yiou, P., & Cattiaux, J. (2013). Contribution of atmospheric circulation to wet north European summer precipitation of 2012. Bulletin of the American Meteorological Society, 94, S39–S41.